CHALMERS
UNIVERSITY OF TECHNOLOGY

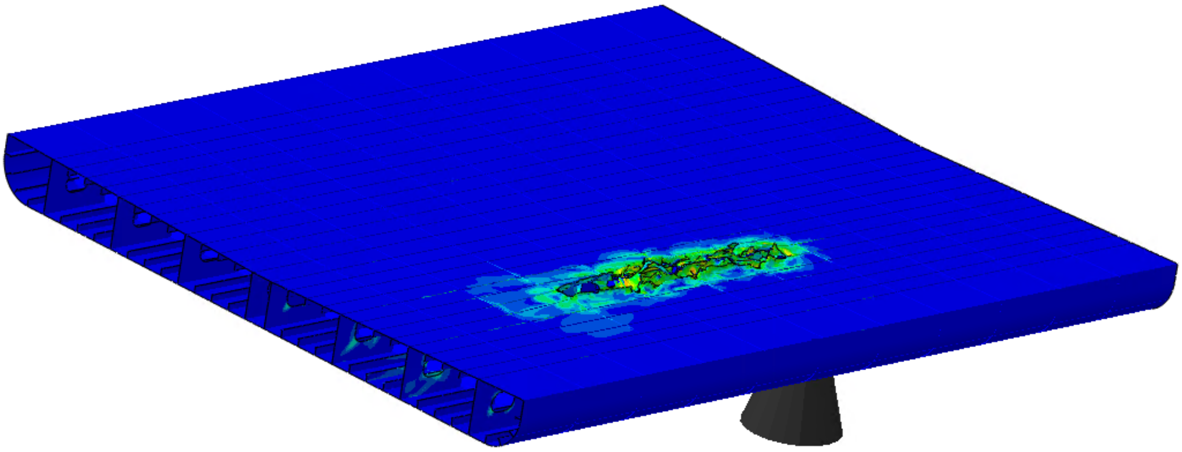

Ultimate limit state of corroded double bottom tanker after grounding events

Master's thesis in the International Master´s Programme in Naval Architecture and Ocean Engineering

ELIN SONESSON

DEPARTMENT OF MECHANICS AND MARITIME SCIENCES

CHALMERS UNIVERSITY OF TECHNOLOGY

Gothenburg, Sweden 2020

www.chalmers.se

MASTER'S THESIS IN THE INTERNATIONAL MASTER'S PROGRAMME IN NAVAL ARCHITECTURE AND OCEAN ENGINEERING

Ultimate limit state of corroded double bottom tanker after grounding events

ELIN SONESSON

Department of Mechanics and Maritime Sciences

Division of Marine Technology

CHALMERS UNIVERSITY OF TECHNOLOGY

Gothenburg, Sweden 2020

Ultimate limit state of corroded double bottom tanker after grounding events

ELIN SONESSON

Master's Thesis 2020:50
Department of Mechanics and Maritime Sciences
Division of Marine Technology
Chalmers University of Technology
SE - 412 96 Gothenburg
Sweden
Telephone: + 46 (0)31 772 1000

Printed by Chalmers Reproservice

Gothenburg, Sweden 2020

Ultimate limit state of corroded double bottom tanker after grounding events
Master's Thesis in the International Master's Program in Naval Architecture and Ocean Engineering
ELIN SONESSON
Department of Mechanics and Maritime Sciences
Division of Marine Technology
Chalmers University of Technology

Abstract

Grounding accidents will inevitably continue to happen, but hopefully the resulting damage can be mitigated by including crashworthiness considerations in the structural design. A lot of research has already been done to investigate the effect of different ground shapes, penetration depths, ship types (e.g. double or single bottom and stiffened or unstiffened structure), collision velocity, and collision position (e.g. under a transverse bulkhead, a longitudinal bulkhead, or an unstiffened plate section).

Typically, the experiments and finite element analyses that are performed are conducted under the assumption that the steel has not succumbed to the harshness of the environment that ships operate in. Therefore, the objective of this thesis is to investigate the effects of corrosion on a structure's resistance to penetration and damage in the event of a ship grounding. Furthermore, the ultimate hull girder strength and residual strength of the hull after various grounding scenarios is investigated.

Nonlinear finite element analysis simulations are conducted in Abaqus/Explicit (Dassault Systèmes, 2020). Displacement controlled grounding simulations are done with two different ground geometries and with three different tanker ages, namely zero, 16, and 25 years. For the aged vessels, the degradation that results from general corrosion is accounted for using two different methods. One method is to just reduce the thicknesses of structural members, while keeping the as-built material properties. The other method is to reduce the thicknesses and to also adjust the constitutive material model so that it more accurately represents the material properties of corroded steel. Reaction forces on the rock are measured during the simulations to determine the impact of adjusting the constitutive material model for the aged tanker models. Ultimate limit state analyses are then carried out with the intact and damaged models to quantify the effects of corrosion on a ship's ultimate hull girder strength.

It is shown that accounting for the material properties of corroded steel is vital to avoid overestimation of the ship's crashworthiness. If the thicknesses are reduced without changing the material model, in some cases, there is less grounding damage compared to the damage seen on the model with a non-corroded material model and full as-built thicknesses. This is especially apparent for the ground geometry with a wide and flat contact area.

Keywords: corrosion, crashworthiness, nonlinear finite element analysis, residual strength, ship grounding, ultimate limit state.

Table of Contents

Abstract I

Table of Contents III

Preface V

List of Acronyms VII

List of Unit Abbreviations VII

Notations VIII

1 Introduction 1

1.1 Background and motivation of study 1

1.2 Review of studies related to ship groundings 3

1.2.1 Analysis of hull bottom damage 3

1.2.2 Ground modeling 4

1.3 Review of ULS methods 5

1.3.1 Smith method 5

1.3.2 Modified Smith method 5

1.3.3 Nonlinear FE bending simulations 6

1.3.4 Calibration of the modified Smith method 6

1.4 Objective and tasks 7

1.5 Limitations and assumptions 7

1.5.1 Ship grounding simulations 7

1.5.2 ULS analyses 8

1.6 Outline of the study 8

2 Tanker FE model and rock geometries 11

2.1 Case study vessel 11

2.2 Finite element model 12

2.2.1 Element size and type 12

2.2.2 Contact conditions 13

2.2.3 Corrosion wastage model 13

2.2.4 Constitutive material and damage models 16

2.3 Rock models 20

3 Grounding and residual strength assessment 23

3.1 Description of parametric study 23

3.2 Grounding simulations 24

3.2.1 Tanker boundary conditions 24

3.2.2 Description of the simulations 25
3.2.3 Outcome of the simulations 25
3.3 Ultimate limit state analyses 26
3.3.1 Biaxial bending 26
3.3.2 Geometry and material modeling for the ULS analyses 28
3.3.3 Residual strength 29
4 Results and discussion 31
4.1 FE grounding simulations 31
4.1.1 Simulation errors 31
4.1.2 Damage openings from select cases 33
4.1.3 Conclusions from grounding cases 36
4.2 Ultimate limit state analyses 40
4.2.1 Ultimate bending moments in intact conditions 41
4.2.2 Reduced ultimate bending moment 42
4.2.3 Conclusions from ULS analyses 44
5 Conclusions 45
6 Future work 47
References 49
Appendix 53
A. Damaged tanker models 53

Preface

The completion of this thesis is a requirement for the master's program in Naval Architecture and Ocean Engineering at Chalmers University of Technology. The work presented herein has been carried out at the Division of Marine Technology, Department of Mechanics and Maritime Sciences, Chalmers University of Technology from January through June of 2020.

First, I would like to thank Professor Jonas Ringsberg, my supervisor and examiner, for his guidance and advice during this project. I also want to thank my supervisor, Artjoms Kuznecovs, for his support, especially for his help with creating the FE model for the grounding simulations and the hull geometries for the ULS analyses.

I would also like to thank my family, friends, and coworkers for their encouragement and support.

Gothenburg June 2020

Elin Sonesson

List of Acronyms

BC	Boundary condition
BL	Baseline
CM	Corrosion margin
CP	Control point
CSR	Common Structural Rules
DE	Damage evolution
DI	Damage initiation
DOF	Degrees of freedom
DWT	Deadweight
FEA	Finite element analysis
FE	Finite element
GBS	Goal-based standards
IACS	International Association of Classification Societies
IMO	International Maritime Organization
MPC	Multi-point constraint
MSC	Maritime Safety Committee
NA	Neutral axis
PSM	Primary supporting member
RSI	Residual strength index
SOLAS	The International Convention for Safety of Life at Sea
STBD	Starboard
ULS	Ultimate limit state

List of Unit Abbreviations

GRT	Gross ton
mm	millimeter
m	meter
N	Newton
MN	Mega Newton
GNm	Giga Newton-meter

Notations

t_c	Corrosion addition	(mm)
t_{as_built}	Actual thickness provided, or as-built thickness	(mm)
t_{off}	Net offered thickness for the as-built condition	(mm)
t_{vol_add}	The thickness voluntarily added as the owner's or builder's extra margin in addition to the required t_c	(mm)
t_{res}	Reserve thickness	(mm)
t_{c1}, t_{c2}	Corrosion additions for each side of the structural member	(mm)
T	Vessel age	(years)
T_c	Effective life of the corrosion inhibitor coating	(years)
C_1	Rate of material wastage	(mm/year)
σ_y	Yield strength	(MPa)
E	Young's modulus	(GPa)
ν	Poisson's ratio	(-)

1 Introduction

The focus of this work is to perform ultimate limit state (ULS) analyses of new and aged ship models after they have been damaged by different grounding events. Section 1.1 begins with some background and motivation of the study. Methods that can be used to simulate ship groundings and to determine the residual strength of the damaged vessel are discussed in Sections 1.2 and 1.3. The sections that follow describe the objective, scope, assumptions, and methodology of this thesis.

1.1 Background and motivation of study

Collisions and groundings have always been factors affecting the maritime industry. Crew and passenger safety, ship survivability, and environmental pollution are major areas of concern with accidents of this nature. The most severe collisions and grounding incidents are typically the catalyst for the development and implementation of more stringent rules that aim to minimize the consequences of future collisions and groundings. The sinking of the RMS *Titanic* is an example of one of the first maritime disasters to drive the development of new regulations. With its double hull construction and individual watertight compartments, the RMS *Titanic* was one of the first vessels to be designed based on damage stability. Yet, its collision resulted in excessive hull damage that led to the loss of 1,522 lives when she sank on April 14, 1912 (Hooper et al., 2003). The international Convention for Safety of Life at Sea (SOLAS) was established two years later, as a direct response to the sinking of the RMS *Titanic*; the objective of this convention was to mandate standards that ultimately reduce damage and casualties in future accidents (IMO, 2020). The *Exxon Valdez* oil spill is another maritime disaster that resulted in new regulations for oil tankers. On March 24, 1989, the *Exxon Valdez* ran aground on Bligh Reef in Prince William Sound, Alaska. The oil tanker was a single hull construction, and its grounding resulted in a hull opening that allowed 41.6 million liters of crude oil to spill into the waters of the Prince William Sound. The outcome of this environmental disaster was the development and enactment of the Oil Pollution Act of 1990, which stipulates that oil tankers operating in US waters must have a double bottom construction (Birkland and Lawrence, 2002).

Even today, grounding accidents make up a big portion of the total losses of vessels greater than 100 gross tons (GRT) (Allianz, 2019). Between the years 2009 and 2018, the annual average number of vessels larger than 100 GRT that have been declared total losses is 104, and as shown in Figure 1.1, grounding accidents constitute approximately 20% of these losses. As shown in Fig. 1.1, the number of total losses decreased by roughly 50% from 2017 to 2018; however, with the increasing size of ships, the risk becomes elevated (Allianz, 2019). Furthermore, among the ten largest ships declared as total losses, are three grounding incidents (Allianz, 2019).

Despite advanced sonar technology and stringent watch-standing regulations, grounding accidents continue to occur. As past events have shown, it is common for the most disastrous of these accidents to drive the development of new regulations that mitigate the consequences of a grounding accident, or possibly reduce the chances of one occurring (Birkland and Lawrence, 2002). While making changes reactively has led to improved safety, adjusting regulations proactively could reduce the likelihood and severity of future accidents without waiting for one of its nature to occur first.

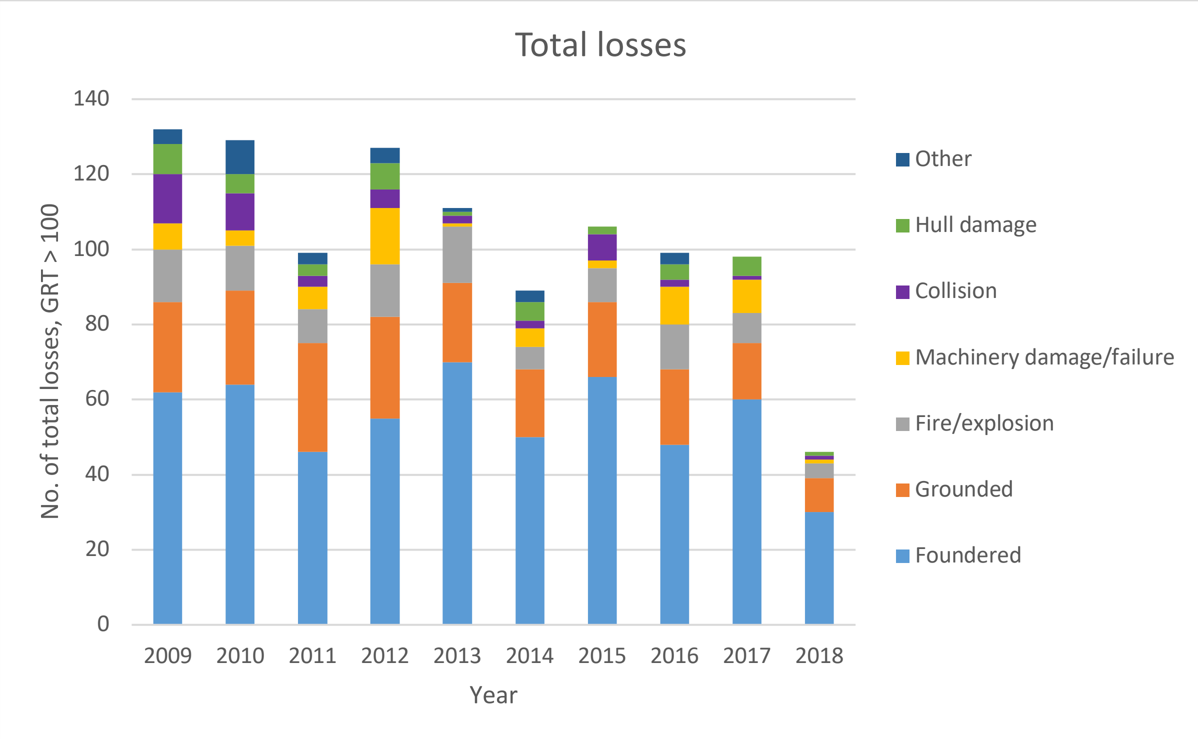

Figure 1.1 Number of total losses of ships with GRT greater than 100 within the years 2009-2018 (Allianz, 2019).

In 2002, during the 89th session of the International Maritime Organization (IMO) Council, the Bahamas and Greece proposed the concept of goal-based ship construction standards with the objective of addressing ship design standards in order to mitigate the risk involved with ship collisions and groundings. The IMO Council referred this proposed concept for consideration to the 77th meeting of the Maritime Safety Committee (MSC), which took place in May and June of 2003. In 2010, during its 87th session, the MSC adopted the Goal-based standards (GBS) and made amendments to Chapter II-1 of SOLAS, making compliance with the GBS a requirement for oil tankers and bulk carriers with a length overall (LOA) of 150 m or greater. As proposed by the Bahamas, Greece, and the International Association of Classification Societies (IACS), and agreed by the MSC, the GBS is comprised of a five-tier system (IMO, 2010). The structure of the system is shown in Table 1.1; all five tiers are outlined in the table, but tiers IV and V have not yet been adopted by IMO's MSC.

The Tier I goals stipulate that, for the duration of their service lives, ships are to be safe and environmentally friendly, both in intact and in certain specified damage conditions (IMO, 2010). Tier II functional requirements have been adopted and defined for bulk carriers and oil tankers; they are in place to ensure that the Tier I goals can be met. As part of the Tier II functional requirements, the ultimate strength must be verified through calculations that show sufficient ultimate hull girder strength and adequate ultimate strength of supporting members (e.g. plates and stiffeners); the environmental conditions that the vessel is designed to operate in are to be taken into account with said calculations (IMO, 2010). Additionally, the Tier II functional requirements stipulate that the hull girder residual strength must be adequate to withstand wave and internal loads in the event of damage resulting from collisions or groundings (IMO, 2010).

Much of the work that comprises this thesis is related to the ultimate and residual hull girder strength requirements of Tier II of the GBS.

Table 1.1 IMO goal-based standards five-tier system structure (IMO, 2010).

Tier I	Goals	High-level objectives to be met.
Tier II	Functional requirements	Criterial to be satisfied in order to conform to the goals.
Tier III	Verification of conformity	Procedures for verifying that the rules and regulations for ship design and construction conform to the goals and functional requirements.
Tier IV	Rules and regulations for ship design and construction	Detailed requirements developed by IMO, national Administrations and/or recognized organizations and applied by national Administrations and/or recognized organizations acting on their behalf to the design and construction of a ship in order to conform to the goals and functional requirements.
Tier V	Industry practices and standards	Industry standards, codes of practice and safety and quality systems for ship building, ship operation, maintenance, training, manning, etc., which may be incorporated into, or referenced in, the rules and regulations for the design and construction of a ship.

1.2 Review of studies related to ship groundings

This section consists of a literature review of previous studies that are related to ship groundings. The summary begins with a review of how hull bottom damage resulting from groundings is analyzed. This is followed by a discussion of ground shape and stiffness modeling.

1.2.1 Analysis of hull bottom damage

This section summarizes some studies that have been done by researchers to further the understanding of the external dynamics and internal mechanics of ship grounding scenarios.

The extent of hull damage that results from a ship grounding incident can be approximated through the use of numerical simulations with large-scale structures, experiments with large-scale structures, and analytical/empirical formulae (Liu et al., 2018). The methods used to estimate hull damage through the implementation of large-scale numerical simulations can be subdivided into two categories. The first is the coupled method, wherein the external dynamics of the rigid hull body and internal mechanics of the hull structure failure are solved simultaneously. This can be done by considering the ship's motions in all six degrees of freedom (6DOF) or by only considering the ship's motions on the waterplane (i.e. surge, sway, and yaw); the latter method is also referred to as the three degrees of freedom (3DOF) coupled method. The second is the decoupled method, which is implemented by treating the external dynamics and internal mechanics separately. With the decoupled method, the external dynamics can be solved using an analytical method such as the one described by Pedersen and Zhang (2000). The internal mechanics are evaluated separately through FEA simulations. In these simulations, it is typical to keep the hull model fixed in space and to move the modeled ground shape along the bottom of the hull with a predefined path and with a constant penetration depth and velocity; this is what was done in the studies performed by Heinvee and Tabri (2015), AbuBakar and Dow (2013), and Simonsen et al. (2009). As described by Liu et al. (2017), the numerical simulation of the grounding event is set to end once the energy absorbed by the structure reaches the value previously determined with the external dynamics analysis.

Yu and Amdahl (2016) performed a study wherein they compared the uncoupled, 3DOF coupled, and 6DOF coupled methods for various ship collision and ship grounding scenarios. The results of their analyses reveal three main findings: 1) The decoupled method can only predict the energy dissipation for the initial impact; 2) Roll, pitch, and heave periodic motions often result in secondary impacts in ship collisions and groundings; 3) The path deviations between the decoupled and coupled methods can be significant, especially for the scenarios with small collision angles. The significance of this is that the decoupled method can, in many cases, predict less severe damage than what would realistically occur. Despite its limitations, the decoupled method is the most commonly used technique used to approximate the hull damage resulting from ship collisions and groundings, simply because it is much quicker and easier to implement.

1.2.2 Ground modeling

Alsos and Amdahl (2007) identified three main types of ground shapes that can be used in grounding simulations, namely rock, reef, and shoal, as shown in Figure 1.2. The different ground geometries were shown to result in different modes of failure, e.g. the rock was shown to cause localized damage in the form of tearing, while the shoal resulted in crushing and global deformations (Alsos and Amdahl, 2007).

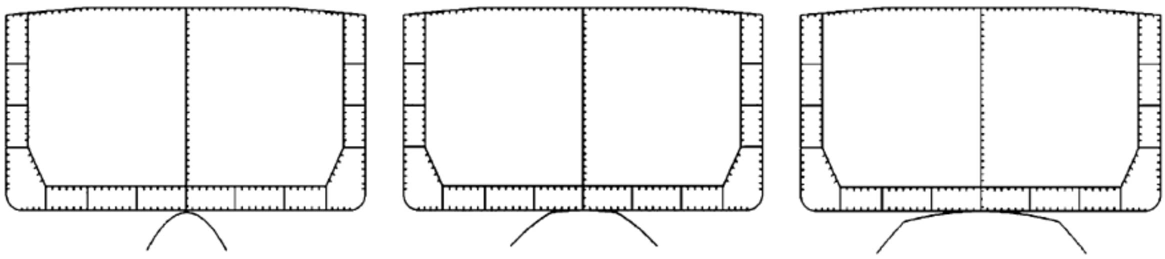

Figure 1.2 Seabed topology: (left) rock, (middle) reef, (right) shoal (Alsos and Amdahl, 2007).

Ship grounding studies are most commonly done with simplified axisymmetric and rigid, non-deformable rock geometries such as the ones identified as rock, reef, and shoal in Figure 1.2; however, Sun et al. (2017) pointed out that these simplified axisymmetric shapes are not an accurate representation of the actual ground topology. Research has been done to develop a method for representing real ground topology with analytical equations (Sormunen et al., 2016); however, the authors of the study showed that a good statistical fit, i.e. an R^2 value close to unity, does not necessarily guarantee an accurate geometrical representation of the real shape and surface. The method described by Sormunen et al. (2016) requires knowledge of the ground topology in the area of service, and is therefore not always practical for ship grounding studies.

Since simple, axisymmetric shapes are not modeled after a particular seabed, grounding simulations with these simplified ground topology models do not yield bottom openings that are representative of a real grounding event. However, the simplified models are sufficient for determining the impact of changing different variables, i.e. the simple rock models allow for generalized conclusions to be made as long as variables are systematically varied such that the effects of each variable can be isolated.

1.3 Review of ULS methods

The ULS of a ship structure is the condition in which it is subjected to the maximum load that it can sustain without collapsing (Paik, 2018). In order to satisfy the requirements of tier II of IMO's GBS described in Section 1.1, it is important to determine the ULS of vessels for a variety of hull conditions and loading cases. The hull girder ultimate bending moment is the most important load to consider when evaluating the longitudinal strength of intact and damaged ships (Fujikubo et al., 2012). A considerable amount of research has therefore been done to develop reliable and practical methods for determining the maximum bending moment that a hull structure can sustain before the onset of progressive collapse; see e.g., Kuznecovs et al. (2020) and Fujikubo et al. (2012), which are based on the method proposed by Smith (1977).

1.3.1 Smith method

The Smith method, adopted by the IACS CSR (IACS, 2020), is an incremental-iterative approach often used because of its ability to generate results rapidly. With this method, each structural member of a hull girder cross section is assigned one of three element types, namely hard corner, stiffener, and stiffened plate. Each element is assumed to act independently, and a stress strain relationship is defined for each structural member, based on its element type. The solution begins with an initial curvature and vertical position of the hull girder section's transverse neutral axis (NA). The next step in the method is to calculate the strain and corresponding stress in each element for the initial curvature. The curvature of the cross section is incrementally increased, and for each curvature increment the new vertical position of the NA is determined from force equilibrium. The corresponding bending moment at each curvature is then found by adding the stress contribution of each element in the cross section. This process is repeated until the bending moment is less than the preceding value. With this method, the vertical position of the NA is considered, but it is always assumed to remain horizontal.

1.3.2 Modified Smith method

For hull girder cross sections that are geometrically symmetrical and that are subjected to purely hogging or sagging loading conditions, the assumption of a horizontal NA is valid; however, if a hull structure is asymmetrically damaged or if it is subjected to asymmetrical loads, a biaxial ULS analysis, wherein the rotation of the NA is considered, is necessary. Fujikubo et al. (2012) proposed amendments to the Smith method that allow for consideration of both the translation and rotation of the transverse NA when determining the ULS for different horizontal and vertical bending moment combinations. Methods for prescribed curvature ratios and prescribed moment ratios were suggested and compared, and they were shown to yield similar results (Fujikubo et al., 2012).

1.3.3 Nonlinear FE bending simulations

Nonlinear FEA techniques have also been developed to predict the bending moment ULS of ship structures; for instance, see the method proposed by Parunov et al. (2018) and Tekgoz et al. (2018). It is possible to create detailed FE hull structure models and to accurately simulate real grounding scenarios in order to generate a realistic damage opening that can then be used in FEA bending simulations to yield accurate results that capture the true failure modes that occur once the ULS is reached. Below is a description of how the method proposed by Parunov et al. (2018) can be implemented in Abaqus/Explicit.

To calculate the hull girder ultimate strength, the FE model is bent with a prescribed curvature rate beyond its bending ULS. Thus, the simulation can capture the progressive collapse of structural members and the different failure modes that occur. Control points (CP) are positioned at the intersection of the initial horizontal NA and the ship's centerline on both the forward and aft planes of the model, see Figure 1.3. The BCs of the FE model's forward and aft ends are controlled with multi point constraints (MPC) with beam elements, i.e., each node on the forward and aft ends is connected via a beam element connected to the forward and aft CP, respectively. Thus, the rotation of each node on the two ends of the model is constrained to whatever is applied to its CP. Bending of the FE model is achieved by applying a linearly increasing rotation angle to the CPs. To allow for pure bending, one of the CPs is pinned and free to move in the longitudinal direction, while it is fixed in the vertical and transverse directions. The other CP is also pinned, but it is restricted from translation in all three directions. The desired biaxial bending condition is achieved by controlling the ratio of CP rotation about the y- and z-axes. The reaction moments at the CPs are measured at every curvature increment while the bending increases. The ULS of the FE model is represented by the maximum recorded bending moment and its corresponding curvature.

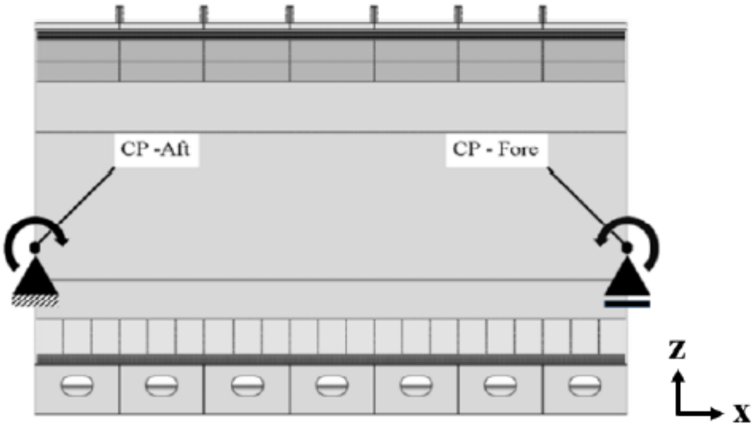

Figure 1.3 Boundary conditions applied to a ship structure during FEA bending simulations (Kuznecovs et al., 2020).

1.3.4 Calibration of the modified Smith method

When results from FEA bending simulations are compared with results from the modified Smith method, they are consistent for vertical bending loads applied to non-corroded and undamaged ship hull structures (Kuznecovs et al., 2020). However, Kuznecovs et al. (2020) showed that the modified Smith method tends to overestimate the maximum bending moment for all cases that are not purely hogging or sagging, especially for corroded and damaged hull structures. While FE based ULS analyses are typically more accurate in their predictions of a ship structure's ULS, these analyses are often impractical due to their computational cost. Kuznecovs et al. (2020) proposed a method that calibrates the Smith method, as modified by Fujikubo et al. (2012), in order to obtain accurate results without the computational cost of running numerous FE simulations. This is done by running a few nonlinear FE bending simulations using the method described in Section 1.3.3 and using the results to calibrate the modified Smith method.

1.4 Objective and tasks

A lot of work has already been done to estimate the shape and size of the hull opening that results from various grounding scenarios. This can be done through numerical simulations, large scale experiments, and analytical methods (Liu et al., 2018). While a lot of research has been done to develop accurate and reliable methods for predicting hull damage that results from grounding events, the main focus has been on new ships that have not yet succumbed to material degradation caused by corrosion. The objective of this thesis is to investigate the importance of material modeling for corroded tankers when addressing Tier II requirements. This is done by investigating the effect of corrosion modeling methods on the ultimate strength of ships, both in their intact and in certain damaged conditions. This objective is achieved through completion of the following tasks:

- Set up and run nonlinear finite element analyses (FEA) of grounding scenarios that result in hull bottom damage of varying shapes and sizes. This is done for both non-corroded and corroded hull materials.
- Perform an ultimate limit state (ULS) analysis and calculate the residual hull girder strength after each grounding scenario. Also perform ULS analyses for the intact non-corroded and corroded hulls.
- Compare and analyze the results to quantitatively determine the reduction in ultimate hull girder strength that results from hull degradation due to corrosion.

1.5 Limitations and assumptions

While the complete midship section shown in Figure 2.1 is used for the ULS analyses, only the double bottom structure is used for the FE grounding simulations. As explained in Section 2.1, the centerline longitudinal bulkhead is neither included in the FE model nor the models for the ULS analyses.

The scope and assumptions for the grounding simulations and ULS analyses are described in Sections 1.5.1 and 1.5.2, respectively.

1.5.1 Ship grounding simulations

The current study has been done with displacement-controlled grounding simulations, i.e. the rock moves along the hull bottom at a constant velocity and penetration depth, and once the prescribed motion has been completed, the simulation ends. Furthermore, the rock is assumed to be rigid, i.e. its shape does not change. This means that energy does not dissipate through deformation of the rock. The boundary conditions (BC) applied to the vessel model are such that the forward and aft ends are fixed in all six DOF, essentially locking the vessel model in space. Furthermore, the length of the rock's path is not determined based on the initial energy of the system; rather, it is made just long enough to have a fully developed damage pattern that spans two frame sections. The exact length not important, as long as the resulting damage is fully developed.

Using just the bottom structure reduces the simulation time to a reasonable length; however, it is possible that the resulting damage is affected due to the reduced stiffness at the sides. It is also likely that the omission of the centerline longitudinal bulkhead affects the deflection, damage pattern, force reactions, and dissipated energy.

In addition to ignoring the external dynamics of the vessel, residual stresses, such as those that result from welding, are not considered in the FE model. It is possible that this simplification could lead to results that indicate less hull damage for a given grounding scenario.

The constitutive material model used to define the failure behavior of the non-corroded hull is based on experimental results from past studies done by other researchers; see Hogström (2012). The available data for the corroded material lack details that describe the necking strain and post necking behavior (Kuznecovs et al., 2020). The plastic hardening of the corroded material is therefore modeled as a linear evolution. Furthermore, it is assumed that the corroded material fails once a certain strain is reached.

For the analyses of the corroded model, the thickness reduction of shell plating is assumed to vary linearly with the vessel's age. The rate of material degradation due to corrosion can range from decreasing to increasing over the span of the structure's service life; however, for simplicity it is common to assume a constant thickness reduction rate once the efficacy of the protective coating is lost (Paik et al., 2003). In order to obtain conservative results that reasonably represent those of corroded steel hulls, it is assumed that the ship's hull, for the duration of its service life, is not re-coated.

1.5.2 ULS analyses

The limitation that arises with using just the double bottom for the grounding simulations is that ULS analyses cannot simply be done as FE simulations with the damaged model. Thus, ULS analyses are done with a Matlab script based on a modified version of the Smith method. The models that are used for these analyses are representative of the complete cross section for the chosen longitudinal position, and they are built up according to the description in Section 3.3.1.

Since the modified Smith method is used for the ULS analyses, the constitutive material models are further simplified by assuming that the steel behaves in a manner that obeys the elastic-perfectly-plastic idealized stress-strain model. For these analyses, the damage propagation and strain hardening are omitted. The plastic deformation of individual supporting members and the residual stresses that result from the grounding incidents are not considered in the calculations of the ULSs. As with the grounding simulations, residual stresses from welding are also not considered for the ULS analyses.

The reduced thickness of aged models is considered in the same way that it is for the grounding simulations.

1.6 Outline of the study

In this parametric study on grounding events, the double bottom of the coastal oil tanker described in Section 2.1 is used; the FE model of the oil tanker's double bottom is described in Section 2.2. Various ground shapes are modeled, and different grounding simulations are set up and executed in order to generate models with different degrees of hull damage and different damage locations. The set-up of the parametric study is described in Section 3.1, and the method used for the grounding simulations is described in Section 3.2. ULS analyses are conducted for the intact non-corroded and corroded models of the complete cross-section of the oil tanker; the methods used are discussed in Section 3.3. The damaged double bottom models that result from the FEA parametric grounding study, are integrated with the tanker's sides and weather deck to obtain complete cross-sections with different degrees of bottom damage. ULS analyses are done to determine the residual hull girder strength. The results of the ULS analyses reveal the effects of corrosion and damage size and on the hull's ultimate and residual hull girder strength. A flowchart outlining the steps and methods involved in the study is shown in Figure 1.4.

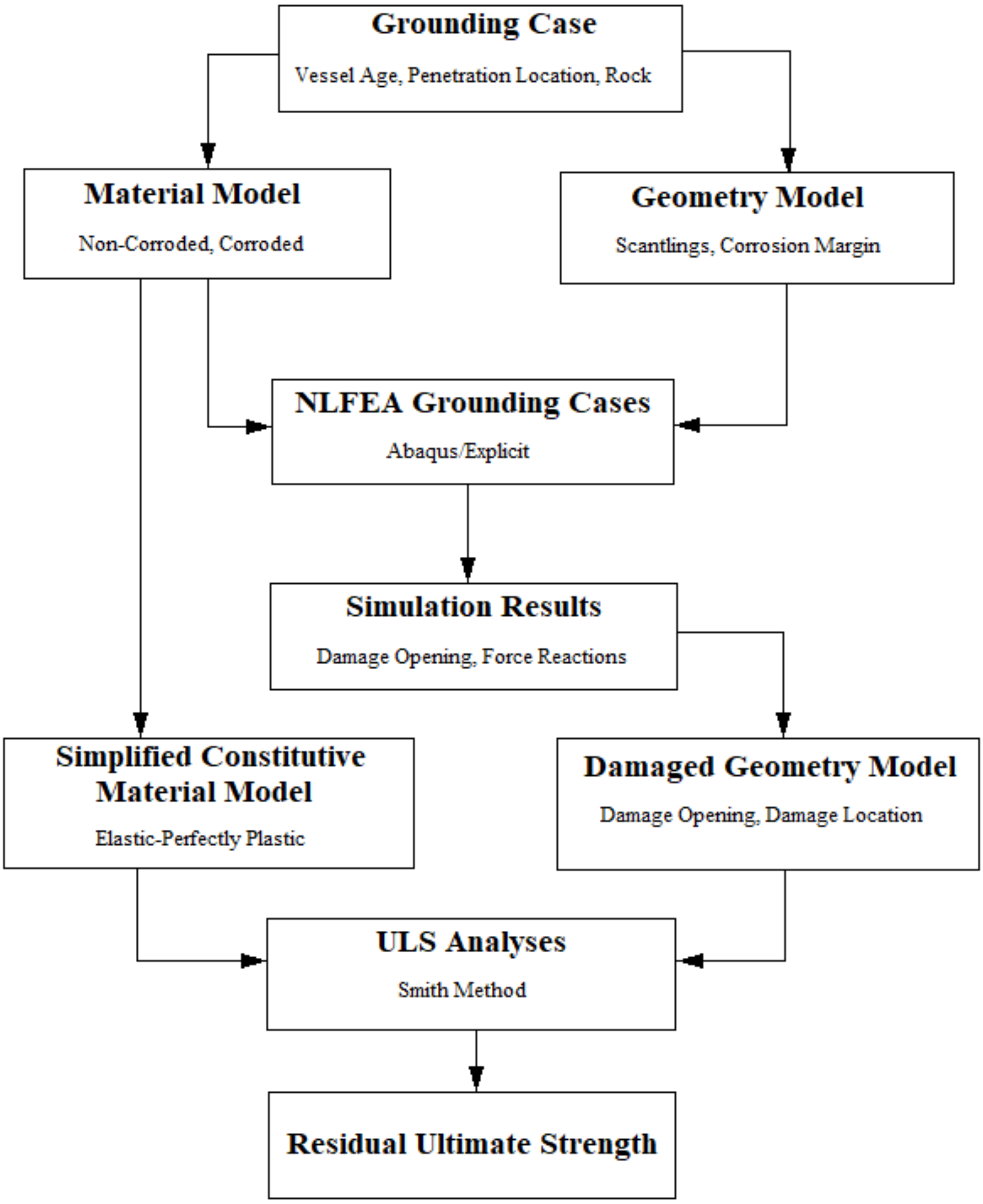

Figure 1.4 Flowchart of the procedure used in the study.

2 Tanker FE model and rock geometries

In this chapter, a description of the case study vessel is first presented. This is followed by a description of the FE model of the vessel, both for its new and aged condition. Finally, Section 2.3 includes a description of the geometry and properties of the rocks used in the grounding simulations.

2.1 Case study vessel

The case study vessel used in the FE simulations and for the ULS analyses is part of an ongoing research project called Structural and Hydro mechanical Assessment of Risk in Collision and grounding (SHARC[1]). It is a coastal oil tanker with a deadweight (DWT) of 11500 tons. The oil tanker's midship section and main particulars are shown in Figure 2.1 and Table 2.1, respectively. The double bottom and weather deck are longitudinally stiffened; however, the double side-shell is transversely stiffened. There is a longitudinal bulkhead located on the vessel's centerline; however, the bulkhead is stiffened with vertical corrugation, and does therefore not contribute significantly to the hull girder's longitudinal bending strength (IACS, 2020). Accordingly, the longitudinal bulkhead is omitted from the FE simulations and the ULS analyses that follow.

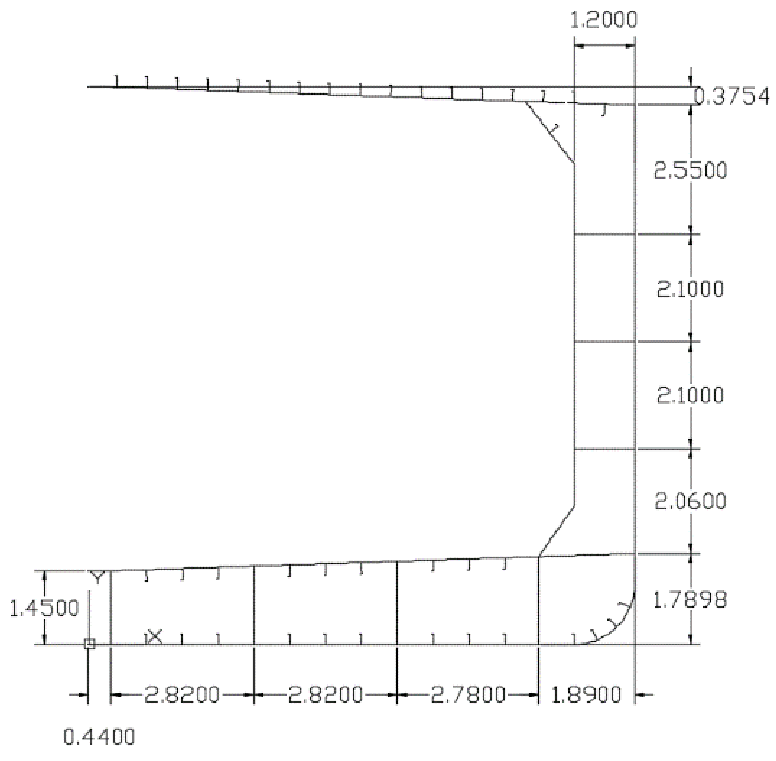

Figure 2.1 Midship section of the coastal oil tanker; units in meters.

Table 2.1 Main particulars of the coastal oil tanker

LOA [m]	Beam [m]	Design draft [m]
137.6	21.5	7.4

[1] https://research.chalmers.se/en/project/?id=9203

2.2 Finite element model

The FE model of the coastal oil tanker is created in Abaqus (Dassault Systèmes, 2020), and is shown in Figure 2.2. The element size and type used for the FE model are described in Section 2.2.1, and the contact definitions are described in Section 2.2.2. Finally, the corrosion wastage and material models are explained in Sections 2.2.3 and 2.2.4, respectively.

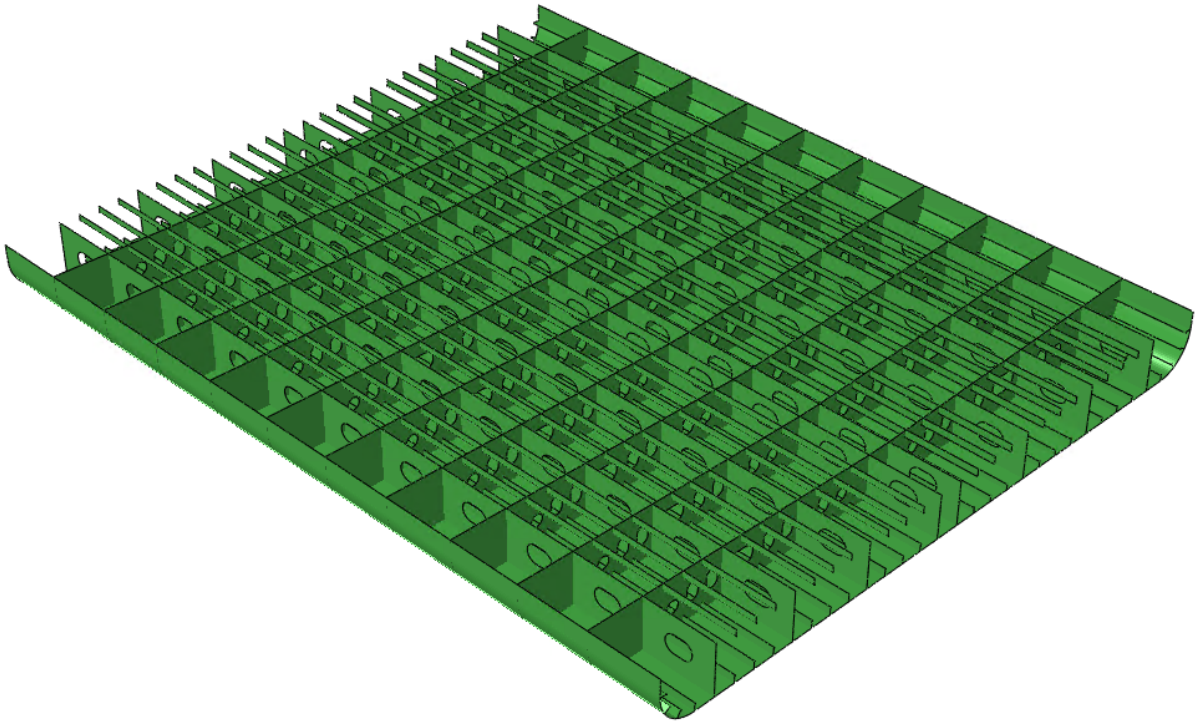

Figure 2.2 FE model of the double bottom structure, with the inner bottom and horizontal bilge girders removed. Note that the mesh is not shown in the model.

2.2.1 Element size and type

The mesh for the FE model consists of four-node shell elements with reduced integration (S4R) and three-node shell elements with reduced integration (S3R). The mesh elements have five integration points through their thickness, and thickness integration is done with Simpson's rule. The element type and the number of through-thickness integration points chosen for the model are the default options available in Abaqus/Explicit (Dassault Systèmes, 2020). Moreover, the mesh is defined in the same way as it is in other studies related to the SHARC project, i.e. the mesh construction is selected based on experience and results from earlier analyses, such as the ones done by Ringsberg et al. (2018) and Kuznecovs et al. (2020). Additionally, this mesh definition was used by other researchers in their FE analyses of ship grounding events, wherein the objective was to determine the extent of the hull damage (AbuBakar and Dow, 2013).

The mesh density is important because the measured strain is sensitive to the element size. Larger elements result in delayed material rupture because strain averaging is done for a larger element area, and thus results in overprediction of maximum reaction forces (AbuBakar and Dow, 2013). Calibration of the FE model is therefore required, and can be done through comparisons of experimental and FE tensile tests along with the implementation of a scaling law such as Barba's relation (Hogström et al., 2009). The mesh convergence studies conducted by Ringsberg et al. (2017) and Hogström and Ringsberg (2011) resulted in an element size of 60 mm. The same model that was used by these authors is used for the grounding simulations in this study; it is thus assumed that a mesh size of 60 mm is also appropriate for these simulations.

2.2.2 Contact conditions

Simonsen (1997) showed that there was good agreement with force reactions when results from the experiments done by Rodd (1997) were compared with results based on a numerical analysis using a friction coefficient of 0.4. However, it is common to use 0.3 as a coefficient of friction for grounding simulations, e.g. see the papers by Heinvee et al. (2016), Heinvee and Tabri (2015), AbuBakar and Dow (2013), and Simonsen et al. (2009). Not a lot of literature can be found on aged ships that have been grounded, but for ship-ship collision simulations, it is common to use a friction coefficient of 0.5 for corroded steel; see Kuznecovs et al. (2020) and Ringsberg et al. (2018). In accordance with the values that are ordinarily assumed in ship-ship collision and grounding simulations, 0.3 and 0.5 are used as the friction coefficients for the FE simulations of the non-corroded and corroded oil tanker model, respectively.

Kuznecovs et al. (2020), Ringsberg et al. (2018), Hogström (2012), and Hogström and Ringsberg (2011) used the Abaqus/Explicit general contact option to define the contact conditions in their FEA studies of ship-ship collisions. Moreover, the same method has been used for the FEA of ship grounding scenarios (AbuBakar and Dow, 2013). With this method of detecting contact between surfaces, contact constraints are enforced with the Abaqus/Explicit penalty option, a method that detects node-face and edge-edge penetrations (Hogström and Ringsberg, 2011). Since previous studies of the coastal oil tanker under consideration have shown successful and consistent results for ship-ship collision simulations using the general contact condition and penalty method available in Abaqus/Explicit, this is also the option used for the FE simulations in the current study on ship groundings.

2.2.3 Corrosion wastage model

Vessels operate in environments that make them susceptible to corrosion. Over time, the thicknesses of shell plating, stiffeners, and primary supporting members (PSM) are reduced due to general or uniform corrosion. During the design of a vessel, corrosion margins (CM) are added to the net scantlings to compensate for the material degradation that occurs over the vessel's service life. The net scantling approach is implemented with the intent that the vessel maintains a minimum required structural strength for the duration of its service life. The first objective of the approach is to give a relationship between the thicknesses used in strengths calculations during the design stage and the minimum allowable thicknesses of structural members during the vessel's service life (IACS, 2020). Its second objective is to allow for evaluation and determination of the structure's status at any given time during the vessel's service life (IACS, 2020). The net offered thickness, t_{off}, is determined as shown in Equation (2.1) (IACS, 2020),

$$t_{off} = t_{as\_built} - t_{vol\_add} - t_c \tag{2.1}$$

where t_{as_built} is the offered thickness of the newbuild, t_{vol_add} is the voluntarily added CM thickness, and t_c is the required CM. Corrosion margins for the oil tanker are determined according to IACS common structural rules (CSR) (IACS, 2020).

The main assumption of the corrosion wastage model used for the study described herein is that the thickness of structural members is inversely proportional to the vessel's age and that the thickness decreases linearly over time once the protective coating has lost its efficacy. The depth of corrosion wastage, t_r, is expressed as a function of time with Equation (2.2) (Paik et al., 2003).

$$t_r = C_1(T - T_c) \tag{2.2}$$

C_1 is the corrosion speed, T is the vessel's age in years, and T_c is the life expectancy of the corrosion inhibiting coating. Based on the study done by Paik et al. (2003), the coating life is assumed to be 7.5 years. The vessel's design life is taken as 25 years, in accordance with the CSR (IACS, 2020). Furthermore, it is assumed that after 25 years, t_r equals t_c, the required CM. The required CM is determined individually for each structural member through the summation of corrosion additions; this is shown with Equation (2.3) (IACS, 2020),

$$t_c = Roundup_{0.5}(\, t_{c1} + t_{c2}) + t_{res} \tag{2.3}$$

where t_{c1} and t_{c2} are the corrosion additions for each side of the structural member and t_{res} is the reserve thickness, and is taken as 0.5 mm. $Roundup_{0.5}(\, t_{c1} + t_{c2})$ means that the summation of the corrosion additions for each side is rounded up to the nearest half millimeter. The rate of corrosion and resulting material wastage depend on environmental factors such as humidity and temperature; corrosion is also dependent on the type of cargo or substance that is in contact with the structural member (Paik et al., 2003). The CSR are used to assign corrosion addition values to shell plating and other structural members. The corrosion addition values are summarized in Table 2.2 (IACS, 2020). The CMs that are used for the oil tanker in the current study are shown in Figure 2.3 and Table 2.3.

With known t_r, T, and assumed T_c, C_1 can be found with Equation (2.4).

$$C_1 = \frac{t_r}{(T - T_c)} \tag{2.4}$$

Equation (2.2) can then be used to estimate the depth of corrosion wastage at any given time in the vessel's service life. It is determined that 50 percent of the required CM has wasted away after the tanker has been in service for 16 years. The thicknesses of the structural members that comprise the as-built, 16-year-old, and 25-year-old oil tankers are shown in Table 2.3.

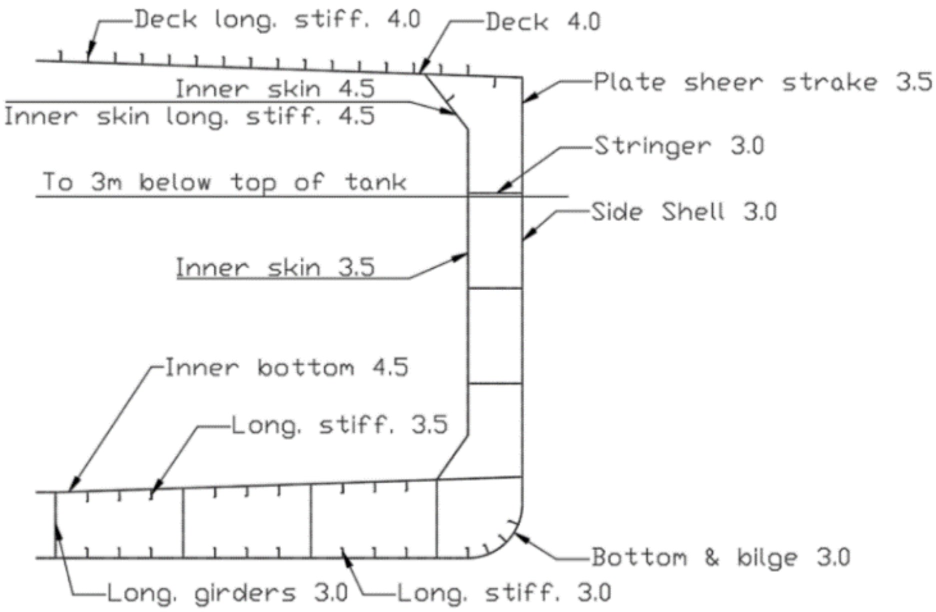

Figure 2.3 Corrosion margin based on location and member type, according to CSR (IACS, 2020).

Table 2.2 Corrosion addition for each side of structural members of oil tankers (IACS, 2020).

Compartment type	**Structural member**		t_{c1} **and** t_{c2}
Ballast water tank, bilge tank, drain storage tank, chain locker	Face plate of PSM	Within 3m below top of a tank	2.0
		Elsewhere	1.5
	Other members	Within 3m below top of a tank	1.7
		Elsewhere	1.2
Cargo oil tank	Face plate of PSM	Within 3m below top of a tank	1.7
		Elsewhere	1.4
	Inner-bottom plating/bottom of tank		2.1
	Other members	Within 3m below top of a tank	1.7
		Elsewhere	1.0
Exposed to atmosphere	Weather deck plating		1.7
	Other members		1.0
Exposed to seawater	Shell plating between the minimum design ballast draft waterline and the scantling draft waterline		1.5
	Shell plating elsewhere		1.0
Fuel and lube oil tank	All		0.7
Fresh water tank	All		0.7
Void spaces	Spaces not normally accessed, e.g. access only via bolted manhole openings, pipe tunnels, inner surface of stool space not common with a dry bulk cargo hold or ballast cargo hold. Etc.		0.7
Dry spaces	Internals of machinery spaces, pump room, storerooms, steering gear space, etc.		0.5

Table 2.3 Corrosion margins and thicknesses at zero, 16, and 25 years of service.

Tanker structural member	**CM [mm]**	**As-built thicknesses [mm]**	**Thicknesses after 16 years [mm]**	**Thicknesses after 25 years [mm]**
Weather deck	4.0	11.0	9.0	7.0
Sheer strake	3.5	11.0	9.25	7.5
Inner shell, 3m below top of tank	4.5	15.0	12.75	10.5
Inner shell	3.5	11.0	9.25	7.5
Inner shell, tank bottom	3.5	13.0	11.25	9.5
Outer shell	3.0	11.0	9.5	8.0
Outer shell, ice belt	3.0	13.0	11.5	10.0
Inner bottom	4.5	12.0	9.75	7.5
Outer bottom and bilge	3.0	11.0	9.5	8.0
Double side stringers	3.0	9.0	7.5	6.0
Double bottom long. girders	3.0	10.0	8.5	7.0
Weather deck long. web	4.0	10.0	8.0	6.0
Weather deck long. flange	4.0	20.0	18.0	16.0
Inner bottom long. web	3.5	10.0	8.25	6.5
Inner bottom long. flange	3.5	20.0	18.25	16.5
Outer bottom and bilge long. web	3.0	10.0	8.5	7.0
Outer bottom and bilge long. flange	3.0	20.0	18.5	17.0
Inner shell long. web	4.5	10.0	7.75	5.5
Inner shell long. flange	4.5	20.0	17.75	15.5
Double bottom side shell frame	3.0	13.0	11.5	10.0
Double wall side shell bottom stiffener	3.0	16.0	14.5	13.0
Double wall side shell middle stiffener	3.0	9.0	7.5	6.0
Double wall side shell top stiffener	4.0	16.0	14.0	12.0
Transverse middle Stiffener flange	3.0	20.0	18.5	17.0
Transverse middle Stiffener web	3.0	10.0	8.5	7.0
Weather deck transverse girder	4.0	10.0	8.0	6.0

2.2.4 Constitutive material and damage models

The material constitutive models for the non-corroded and corroded hulls are described in this section.

2.2.4.1 Non-corroded material

The oil tanker is constructed with NVA shipbuilding mild steel (Ringsberg et al., 2018). The material properties of this steel are shown in Table 2.4. The behavior of the material is captured with a non-linear elastic-plastic constitutive model wherein the isotropic hardening in the inelastic region is described by Equation (2.5),

$$\sigma_{true} = K(\varepsilon_{true})^n \tag{2.5}$$

where σ_{true} and ε_{true} are the true stress and strain, respectively; K and n are the material's hardening coefficient and hardening exponent, respectively. Strain rate effects are accounted for with the Cowper-Symonds relation shown in Equation (2.6),

$$\sigma_{y,d} = \sigma_{y,s}\left(1 + (\dot{\varepsilon}/C)^{1/P}\right) \tag{2.6}$$

where $\sigma_{y,d}$ is the dynamic yield stress, $\sigma_{y,s}$ is the static yield stress, $\dot{\varepsilon}$ is the strain rate, and C and P are constants of the Cowper-Symonds relation.

In order to model the material degradation and fracture during the grounding simulations, damage initiation (DI) and damage evolution (DE) models are used. The DI represents the onset of necking, or the point at which failure starts to occur. In order to model DI, the shear criterion in Abaqus/Explicit is used. The shear criterion, as it is implemented in Abaqus/Explicit, is a representation of damage initiation resulting from shear band localization. The material degradation after the onset of necking is represented with the DE model. For this post necking region, the fracture strain becomes sensitive to the element size. The dependency of fracture strain on the element size must therefore be considered in the definition of the DE model. As it has been shown by Hogström et al. (2009) that Barba's law can be used for this purpose, that is also the method used in the current study. Furthermore, a bilinear law is applied to the DE model, based on the recommendations made by Hogström et al. (2009).

Table 2.4 Material parameters used for the non-corroded model (Ringsberg et al., 2018).

Parameter	As-built NVA steel
Young's modulus, E (MPa)	210 000
Poisson's ratio, ν (-)	0.3
(Static) Yield stress, $\sigma_{y,s}$ (MPa)	310
Ultimate tensile strength (MPa)	579
Hardening coefficient, K (MPa)	616
Hardening exponent, n	0.23
Necking strain, ε_n (%)	23.0
Fracture strain, ε_n (%)	35.1
Cowper-Symonds constant, C (-)	40.4
Cowper-Symonds constant, P (-)	5
DE parameters, bilinear model	(0,0), (0.02,0.00458), (1,0.01832)

2.2.4.2 Corroded material

The constitutive material models used in the current study to represent the corroded steel's properties are the same as the ones used in Ringsberg et al. (2018), wherein the method proposed by Garbatov et al. (2014) was used to obtain the corroded hull's material parameters. It was concluded, in their study, that a steel specimen's elastic properties and yield point are related to the amount of material wastage that results from corrosion. In their study, empirical formulas were derived from the results of standard tensile tests of four different corroded steel specimens, wherein the percentage of material degradation was related to Young's modulus and yield stress (Garbatov et al., 2014). Equation (2.7) shows the derived empirical formula that can be used to determine Young's modulus (E) as a function of the degree of material degradation.

$$E(D) = -1.0349D + 196 \quad \text{GPa} \tag{2.7}$$

In Equation (2.7), D is the degree of material degradation, and is expressed as a percentage of the specimen's volume reduction from its new to corroded state. This is shown in Equation (2.8),

$$D = \frac{V_0 - V_c}{V_0} \times 100\% \tag{2.8}$$

where V_0 is the volume of the non-corroded specimen, and V_c is the volume of the corroded specimen. The empirical formula that relates the degree of corrosion related material degradation to yield stress (σ_y) is shown in Equation (2.9).

$$\sigma_y(D) = -0.0229D^2 + 0.5551D + 235 \quad \text{MPa} \tag{2.9}$$

In their study, steel specimens that were 20, 40, 60, and 80 percent corroded were used to obtain four material constitutive models that correspond with the four degrees of material degradation; the stress-strain relationships for the four materials are shown in Figure 2.4.

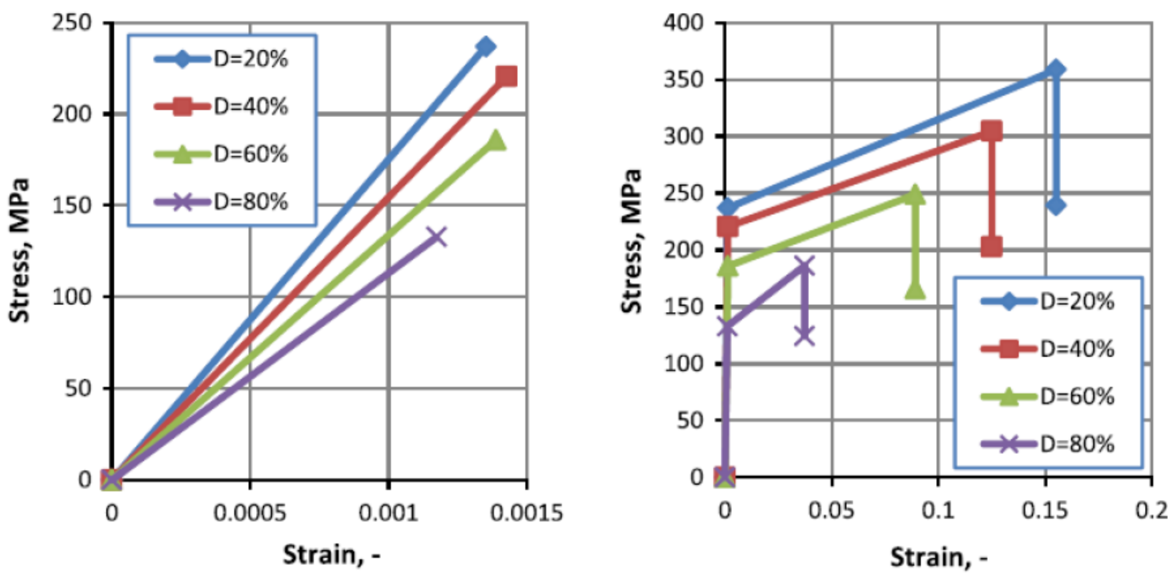

Figure 2.4 Linear elastic (left) and bilinear elastic-plastic (right) stress-strain relationship for four levels of corrosion (Garbatov et al., 2014).

In the current study, the areas of the shell elements that comprise the FE model are constant, regardless of the thickness reduction that results from corrosion. Equation (2.8) is thus simplified as follows:

$$D = \frac{t_r}{t_{as\_built}} \times 100\% \tag{2.10}$$

In Equation (2.10), t_{as_built} is the as-built thickness, and t_r is the difference in thickness of the new and corroded plates.

As explained in Section 2.2.3, the CSR guidelines summarized in Table 2.2 are used to determine the required CM for structural members in different parts of the model; the resulting CMs for PSMs and other structural members in different locations of the model are summarized in Figure 2.3 and Table 2.3. For the 25-year-old model, the full CM thicknesses are subtracted from the as-built thicknesses to determine t_r. To determine t_r for the 16-year-old model, only 50% of the required CM thicknesses shown in Figure 2.3 are subtracted from structural members. Equation (2.10) is then used to determine the degree of corrosion for each member. Since the study done by Garbatov et al. (2014) yielded material models only for 20, 40, 60, and 80 percent corroded steels, the material model used for a particular member is based on the corrosion percentage interval that *D* happens to fall within. Table 2.5 shows the corrosion intervals and corresponding material models used in the current study.

Table 2.5 Material model assignment based on corrosion percentage range.

Corrosion Percentage (*D*)	Material Model
0 ~ 9%	NVA – Non-corroded
10 ~ 29%	NVA 20% Corroded
30 ~ 49%	NVA 40% Corroded
50 ~ 69%	NVA 60% Corroded
70 ~ 89%	NVA 80% Corroded

Since the steel used in the study done by Garbatov et al. (2014) is not the same as the NVA shipbuilding steel used for the tanker model in the current study, material models needed to be created for the varying degrees of corrosion seen in different parts of the model. Young's modulus, ultimate tensile strength, and failure strain are read from Figure 2.4 for the four different corrosion percentages. These values were compared with the corresponding values for the non-corroded material used in the study performed by Garbatov et al. (2014) in order to determine percent change for each degree of corrosion. These percentage reductions were then applied to the non-corroded NVA shipbuilding steel to obtain material models for varying degrees of corrosion.

After applying the appropriate CM thickness reductions for the 16 and 25-year-old models, it was determined, using Equation (2.10), that all corrosion percentages fall below 49%. Therefore, only two constitutive material models are needed to represent the varying degrees of corrosion of NVA shipbuilding steel; see Table 2.6. The material model for severe corrosion is used in parts of the hull that have corrosion in the range of 30 to 49%. For the parts of the hull that are between 10 and 29% corroded, the material model for minor corrosion is used. The parameters that comprise the constitutive material models for the two degrees of corrosion are shown in Table 2.6.

Unlike the nonlinear constitutive material model used to represent the non-corroded steel, the constitutive material models that represent the two corroded materials are bilinear and elastic-plastic. Another difference is that the isotropic hardening in the inelastic region between the start of plastic deformation and the onset of necking is linear. Furthermore, the Cowper-Symonds relationship could not be applied due to a lack of necessary material data; effects from strain rate are therefore not considered for the corroded materials, as they are for the non-corroded material.

Table 2.6 Material parameters used for the corroded model (Ringsberg et al., 2018).

Parameter	NVA steel, minor corrosion	NVA steel, severe corrosion
Young's modulus, *E* (MPa)	179	158
Poisson's ratio, ν (-)	0.3	0.3
(Static) Yield stress, $\sigma_{y,s}$ (MPa)	310	291
Ultimate tensile strength (MPa)	518	440
Hardening coefficient, *K* (MPa)	845	752
Hardening exponent, *n*	1.00	1.00
Necking strain, ε_n (%)	-	-
Fracture strain, ε_n (%)	24.8	20.0
Cowper-Symonds constant, C (-)	-	-
Cowper-Symonds constant, P (-)	-	-
DE parameters, bilinear model	-	-

Since corrosion reduces the ductility of a material, it is difficult to observe and accurately determine the elongation at the onset of necking when corroded steel specimens are used in uniaxial tensile tests (Garbatov et al., 2014). Therefore, the model that is used in Abaqus/Explicit to mimic the degradation and failure of the corroded material is altered from that of the non-corroded model. The shear failure criterion is still used as the DI model to identify the onset of necking; however, the bilinear DE law that is used to describe the degradation of the non-corroded material between the necking and fracture points, is not used for the corroded damage model.

2.3 Rock models

The two rocks that are used in the grounding simulations are shown in Figure 2.5. Geometrically, they were designed based on the "rock" and "reef" in Figure 1.2. The dimensions were chosen so that one rock would have a small contact area and the other a large contact area, since these two shapes result in different failure mechanisms and damage openings. The rocks were made sufficiently tall to ensure that their bases would not affect the grounding damage. The rocks are modeled as 3D analytical rigid shell parts. Each rock geometry is assigned an analytical surface and a reference point. Using the analytical surfaces and the reference points, rigid body constraints are created for the rocks. This definition of the rocks allows for the use of the general contact interaction and the penalty method. It also allows for BCs to be applied directly to the rock's reference point, since the reference point is associated with the analytical surface, by means of the rigid body constraint. Note that the rock models are non-deformable since they are modeled as rigid parts with rigid body constraints.

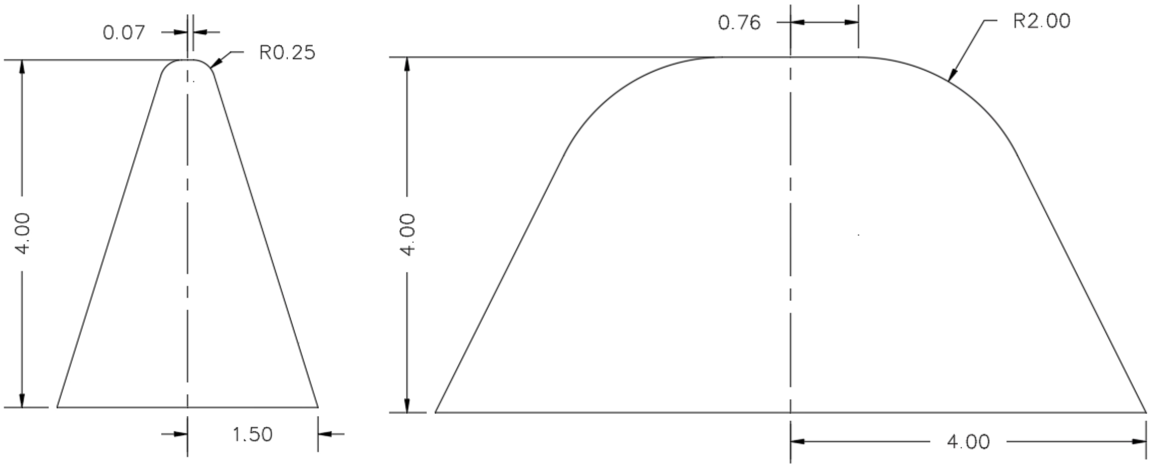

Figure 2.5 Rock geometries used for the grounding simulations; (left) and (right) modeled as "rock" and "reef", respectively. Units in meters.

3 Grounding and residual strength assessment

This chapter begins with a description of the parametric study of the grounding simulations. The methods used for the grounding simulations and ULS analyses are described in Sections 3.2 and 3.3, respectively.

3.1 Description of parametric study

In order to quantitatively determine the effects of corrosion and corrosion modelling methods on the ultimate and residual hull girder strength of the studied oil tanker, one oil tanker is studied at three different stages of its service life, namely after zero, 16, and 25 years of service. These three ages correspond with three different steel thicknesses and material properties. Variables such as the material constitutive model, the CM reduction, rock geometry, and penetration location are systematically varied to determine the effects of each. The grounding simulations that are part of this parametric study are shown in Table 3.1 and the rock shapes and positions are shown in Figure 3.1.

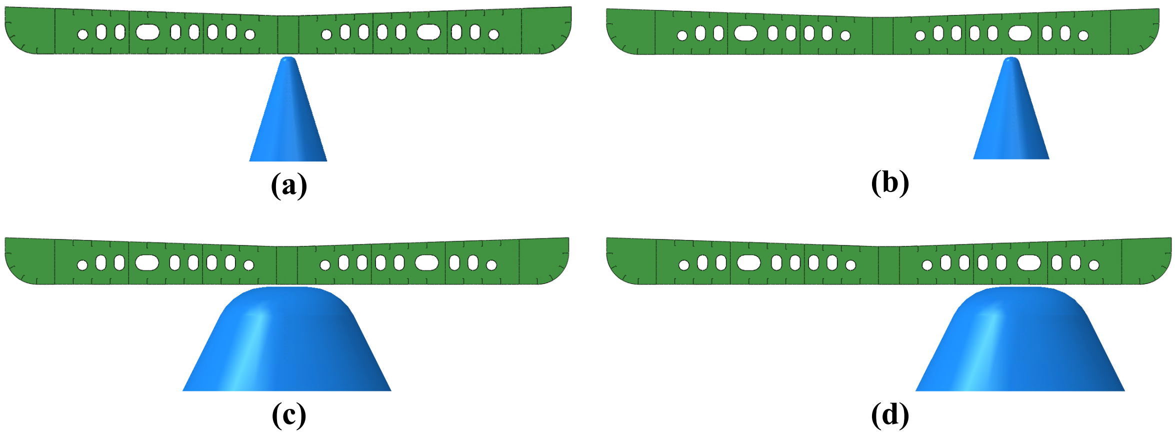

*Figure 3.1 Shape and position of the rock. **(a)** Narrow, centerline; **(b)** narrow, 1/4B; **(c)** wide, centerline; **(d)** wide, 1/4B.*

For all simulations, the rock's motion is parallel to the tanker's centerline plane and a velocity of 5 knots and a penetration depth of 2 m are used. The rock is moved 8 m in the longitudinal direction during the horizontal step to ensure that a fully developed damage pattern is achieved. The two penetration locations shown in Figure 3.1 are chosen because the hull structure is different in those two locations, and it is interesting to see how the different structures affect the results. It is also of interest to see how asymmetrical and symmetrical damages affect the ULS differently. The two rock geometries are selected to see if corrosion considerations are more important for one type of ground topology than another.

For the cases with the as-built, or new hull structure, the friction coefficient is 0.3 and the constitutive material model is the non-corroded model. For the simulations with the aged model, the material thickness is varied by subtracting the thickness obtained with Equation (2.2) from the as-built thickness. That is, for the 16-year-old and 25-year-old vessels, 50 and 100 percent of the CM is subtracted from the as-built thickness, respectively. The constitutive material models described in Section 2.2.4 are used for the cases with the aged ship. To separate the effects of the corroded constitutive material models from the effects of the reduced CMs, cases wherein the thicknesses are reduced without changing the material model are also tested. For the aged model, a friction coefficient of 0.5 is used, regardless of the method used to model the condition of the steel.

Table 3.1 Grounding simulations included in the parametric study.

Case	Material model	CM reduction [%]	Friction coefficient	Penetration location [m]	Rock shape
T-AB-1	Non-corroded	0	0.3	Centerline	Narrow
T-AB-2	Non-corroded	0	0.3	1/4B	Narrow
T-AB-3	Non-corroded	0	0.3	Centerline	Wide
T-AB-4	Non-corroded	0	0.3	1/4B	Wide
T-C50-1	Minor corrosion	50	0.5	Centerline	Narrow
T-C50-2	Minor corrosion	50	0.5	1/4B	Narrow
T-C50-3	Minor corrosion	50	0.5	Centerline	Wide
T-C50-4	Minor corrosion	50	0.5	1/4B	Wide
T-C50-5	Non-corroded	50	0.5	Centerline	Narrow
T-C50-6	Non-corroded	50	0.5	1/4B	Narrow
T-C50-7	Non-corroded	50	0.5	Centerline	Wide
T-C50-8	Non-corroded	50	0.5	1/4B	Wide
T-C100-1	Severe & Minor	100	0.5	Centerline	Narrow
T-C100-2	Severe & Minor	100	0.5	1/4B	Narrow
T-C100-3	Severe & Minor	100	0.5	Centerline	Wide
T-C100-4	Severe & Minor	100	0.5	1/4B	Wide
T-C100-5	Non-corroded	100	0.5	Centerline	Narrow
T-C100-6	Non-corroded	100	0.5	1/4B	Narrow
T-C100-7	Non-corroded	100	0.5	Centerline	Wide
T-C100-8	Non-corroded	100	0.5	1/4B	Wide

3.2 Grounding simulations

In this parametric study on grounding events of non-corroded and corroded ships, the double bottom of the coastal oil tanker described in Section 2.1 is used; the FE model of the oil tanker's double bottom is described in Section 2.2.

3.2.1 Tanker boundary conditions

Multi-point constraints (MPC) with beam elements are applied to both ends as a means of implementing fully fixed BCs; see Figure 3.2. Nodes along the perimeter of the model's forward and aft ends are selected and saved as forward and aft node sets. CPs are made and placed at the geometrical centers of the forward and aft ends of the FE model. The forward and aft MPCs are applied by selecting the node sets as the slave elements and the CPs as the master elements. Thus, the forward and aft CPs govern the BCs applied to the FE model's forward and aft ends, respectively, i.e. the rotation and translation of each node is constrained to that of its corresponding CP.

For the constant displacement grounding simulations that were done in this study, it would also be possible to apply fixed BCs directly to each node on the forward and aft faces. While the results would be the same with this type of a definition for the grounding simulations in this study, MPCs are useful because they allowed for a simplified process for other simulations, e.g. the bending simulation described in Section 1.3.3.

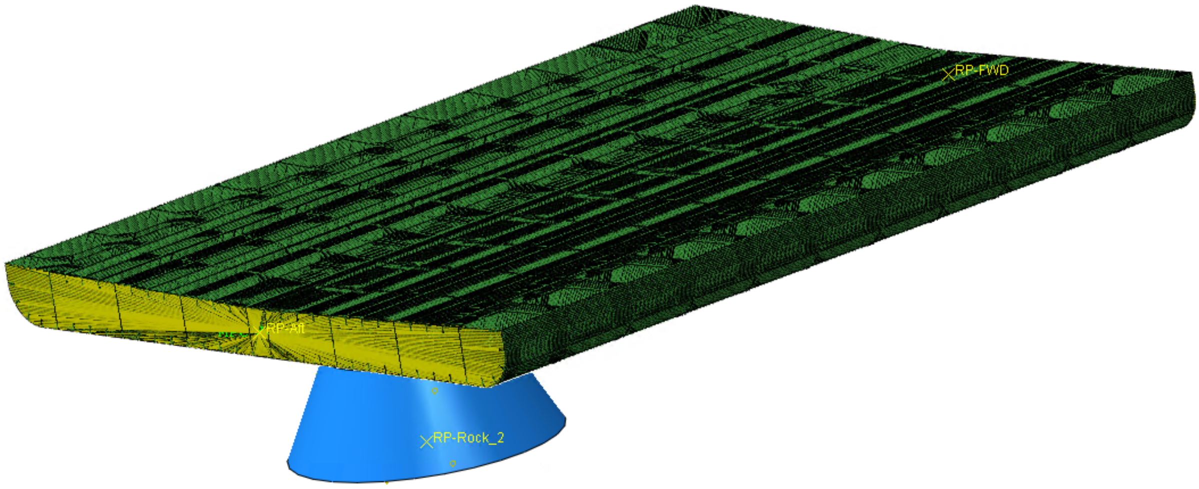

Figure 3.2 Double bottom FE model with multi-point constraints and the wide rock with its reference point.

3.2.2 Description of the simulations

The two rocks described in Section 2.3 are used in the grounding simulations. For each case, the rock's path is such that it penetrates the hull bottom at an angle of 45° with the baseline (BL). Once the desired penetration depth is reached, the rock's vertical motion ends. The rock then moves at a constant penetration depth in the longitudinal direction until the desired damage length has been reached, i.e. until it has moved 8 m. The rock is then retracted from the hull bottom, also at an angle of 45° to the BL. The rock penetrates the hull bottom at 45° to avoid numerical errors, although it is seen in Section 4.1.1 that sudden spikes or drops in reaction forces remain for several simulations. For all three steps, the rock moves at 5 knots since this is generally considered slow enough to limit strain rate effects (Liu and Soares, 2016). The rock's path and speed are specified in Abaqus/Explicit by defining three individual steps: penetration, horizontal, and retraction. Displacement BCs are applied to the rock's CP; see Section 2.3 for a description of how this works. The BCs are changed in each step to make the rock follow the prescribed path. The rock's speed is controlled simply by assigning a length of time to each step and by applying a linearly increasing shape function (i.e. the tabular amplitude in Abaqus/Explicit) to the rock's displacement BCs. The tabular amplitude ensures that the rock's displacement increases linearly so that its velocity is constant during a given step.

The model that is used to estimate the degree of material degradation due to corrosion is described in Section 2.2.3. The constitutive and material damage models that are used to define the point of element deletion from the FE model, are explained in Section 2.2.4.

3.2.3 Outcome of the simulations

The results that are of interest in the grounding simulations are the vertical and horizontal reaction forces on the rock, and the damage size and failure mechanism in the bottom structure. The force reaction is of interest because it is an indicator of how resistant the structure is to material rupture. Higher reaction forces indicate that the structure can sustain higher contact forces before rupturing; higher reaction forces also indicate that for a given initial vessel speed, the damage length is shorter, since the area under the force-displacement curve is equivalent to the energy determined from the external dynamics analysis. In this study, the external dynamics of the vessel were not studied, but as a rough approximation, it can be assumed that 100 percent of the ship's initial kinetic energy is dissipated through deformations of the structure, i.e. internal energy and friction. In Abaqus/Explicit, the internal energy is broken down into energy from elastic and plastic deformations and energy dissipated during impact. Thus, it is assumed that the vessel's initial kinetic energy is equivalent to the integrated reaction force over the rock's path. Thus, higher dissipated energy - travelled distance ratio is associated with improved crashworthiness.

3.3 Ultimate limit state analyses

When sailing in head or following seas, ships are subjected to mainly vertical longitudinal bending moments that result from the superposition of the ship's weight distribution and the buoyant force distribution from still water and waves. This loading condition results in a purely hogging or sagging condition, depending on the net vertical longitudinal bending moment distribution. However, in the event of oblique waves, parametric rolling, or asymmetrical hull damage, the ship is subjected to both vertical and horizontal bending moment components. The oil tanker's ultimate hull girder strength is therefore assessed by simulating scenarios that induce biaxial bending moments. This is done with a Matlab script developed by Kuznecovs and Shafieisabet (2017). The method used to determine the biaxial bending ULS of the tanker is described in Section 3.3.1. For an explanation of how the damaged cross sections are modeled, see Section 3.3.2.

The reduction in the oil tanker's bending ULS due to corrosion, damage, or a combination of the two is evaluated with the residual strength index (RSI), and the method used to calculate this value is discussed in Section 3.3.3.

3.3.1 Biaxial bending

The Smith method (Smith, 1977), as modified by Fujikubo et al. (2012) is implemented in the program, which from now on is referred to as the URSA code. One feature of the URSA code is that it is also able to calculate a hull girder's bending ULS with the calibration method proposed and verified by Kuznecovs et al. (2020). However, only the modified Smith method is used for the ULS calculations since nonlinear FE bending simulations were not done.

The Smith method that was further developed by Fujikubo et al. (2012) is an incremental method that can be implemented for simple ULS analyses of hull girders subjected to biaxial bending moments. With this method, it is assumed that warping does not occur, and thus the method cannot be used for ULS analyses of hull girders subjected to torsional loads. In order to use the method, the structural components of the cross section must be split into three categories: hard corner element, stiffener element, and stiffened plate element. The element types are described in Section 3.3.2. The stress-strain relationship of each structural member is governed by a load shortening elongation (LSE) curve, which is assigned based on the element type. The LSE curves that were defined in the URSA code were done so based on the semi numerical expressions in the CSR (IACS, 2020). For each element, the average stress in the ship's longitudinal direction is thus dictated by the stress-strain relationship of its LSE curve.

In the modified Smith method used in this study, the curvature of the frame section was incrementally increased by bending the structure under a prescribed moment ratio. The horizontal and vertical reaction moments were solved at each curvature increment through integration of the longitudinal stress-strain ratios of all the elements in the cross section. For each curvature, the rotation and translation of the NA was determined, and its instantaneous position was used in the integration of the element stiffnesses. This was achieved by solving a system of nonlinear equations at each increment. The equations are as follows:

$$\begin{Bmatrix} \alpha\Delta M_V \\ \Delta M_V \end{Bmatrix} = \begin{bmatrix} D_{HH} & D_{HV} \\ D_{VH} & D_{VV} \end{bmatrix} \begin{Bmatrix} \Delta X_H \\ \Delta X_V \end{Bmatrix} = \boldsymbol{D} \begin{Bmatrix} \Delta X_H \\ \Delta X_V \end{Bmatrix} \tag{3.1}$$

where $\alpha = \Delta M_H / \Delta M_V$, ΔX_H and ΔX_V are the horizontal and vertical curvature components, respectively, and $\boldsymbol{D}$ is the tangential stiffness, or longitudinal stress-strain ratio matrix. The tangential stiffness matrix, $\boldsymbol{D}$, for the cross section at the j-th curvature increment, is comprised of the following components:

$$D_{VV} = \sum_{i=1}^{N} D_i \, (z_i - z_G)^2 A_i \tag{3.2}$$

$$D_{HH} = \sum_{i=1}^{N} D_i \, (y_i - y_G)^2 A_i \tag{3.3}$$

$$D_{HV} = D_{VH} = \sum_{i=1}^{N} D_i \, (y_i - y_G)^2 (z_i - z_G)^2 A_i \tag{3.4}$$

In Equations 3.2 through 3.4, A_i is the cross sectional area of the i-th element and y_i and z_i and y_G and z_G are the coordinates of the element's and the cross section's centroids, respectively. For the j-th curvature increment, the stiffness, D_i, is the slope of the LSE curve at instant strain of the i-th element. N is the total number of elements in the cross section. For every curvature increment, the coordinates of the instantaneous NA were calculated with the following equations:

$$y_G = \frac{\sum_{i=1}^{N} D_i A_i y_i}{\sum_{i=1}^{N} D_i A_i} \qquad z_G = \frac{\sum_{i=1}^{N} D_i A_i z_i}{\sum_{i=1}^{N} D_i A_i} \tag{3.5}$$

For each increment j, the curvature and horizontal and vertical bending moments were added to the corresponding values found at all previous increments. The ULS for a given loading condition was then identified as the maximum bending moment. For each intact and damaged cross section, this process was repeated for several values of α, and for every α, the maximum bending moment was plotted in a biaxial plot, such as the one shown in Figure 3.3. The bending load ratios, i.e. α, are shown in degrees, and the corresponding bending ULS is the vector from the origin of the polar plot to the recorded value.

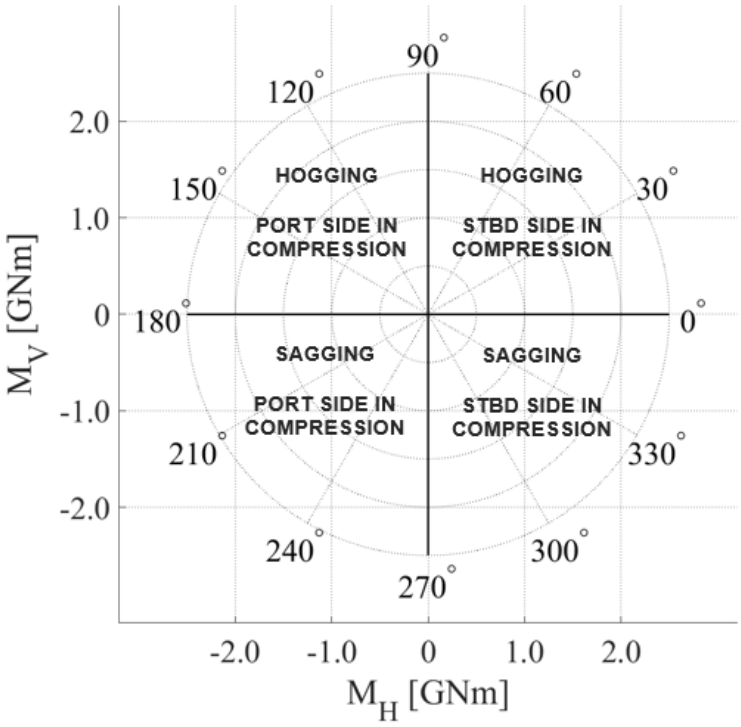

Figure 3.3 Definition of ULS bending moment ratios in a biaxial polar plot.

3.3.2 Geometry and material modeling for the ULS analyses

In order to use the URSA code to evaluate the bending ULS, models of the oil tanker cross section needed to be created. Structural members were defined according to their element type, as specified in the Smith method (Smith, 1977). As mentioned in Section 3.3.1, the three types of elements are hard corner, stiffener, and stiffened plate.

Hard corner elements are typically assigned to areas where there are intersecting plates that lie in different planes. A hard corner element is assumed to be stiff, and its failure mode is defined by an elasto-plastic collapse, i.e. structural members that are put in this category of element types only fail by yielding, not buckling.

Stiffener elements are assigned to parts of the hull structure cross section that are longitudinally stiffened. This element type is made up of the longitudinal stiffener and the shell plating attached to it.

Stiffened plate elements are assigned to plating that is transversely stiffened or plating between hard corners and stiffener elements.

The modeling of the damage opening was done by considering the second to last frame section that was fully damaged during the horizontal step of the grounding simulation. Elements in the FE model that were severely distorted or ruptured during the grounding simulation were removed or adjusted in the URSA code model. For the elements that were adjusted, their LSE curves were modified accordingly. See Appendix B for cross sections of all the damaged models that were used in the URSA code.

As with the FE model for the grounding simulations, material models for structural members with minor and severe corrosion were assigned as shown in Figure 3.4. As explained in Section 1.5.2, the material properties were simplified, and defined such that the materials behave in a manner that obeys the elastic-perfectly-plastic stress-strain relationship. This was done in accordance with the CSR (IACS, 2020). This assumption allows for realistic results in the elastic and ultimate regions; however, that is not the case after the onset of necking. The material properties used to represent the three different conditions of the elastic-perfectly plastic steel are shown in Table 3.2; these values are taken from Tables 2.4 and 2.6. For the new tanker and the aged tankers wherein only the CM reduction method was used, all parts of the hull were assigned the as-built NVA steel material.

Table 3.2 Material properties used for the ULS analyses.

		As-built NVA	Minor corrosion	Severe corrosion
Yield strength, σ_y	[MPa]	310.0	310.0	291.0
Young's modulus, E	[GPa]	210.0	179.0	158.0
Poisson's ratio, ν	[-]	0.3	0.3	0.3

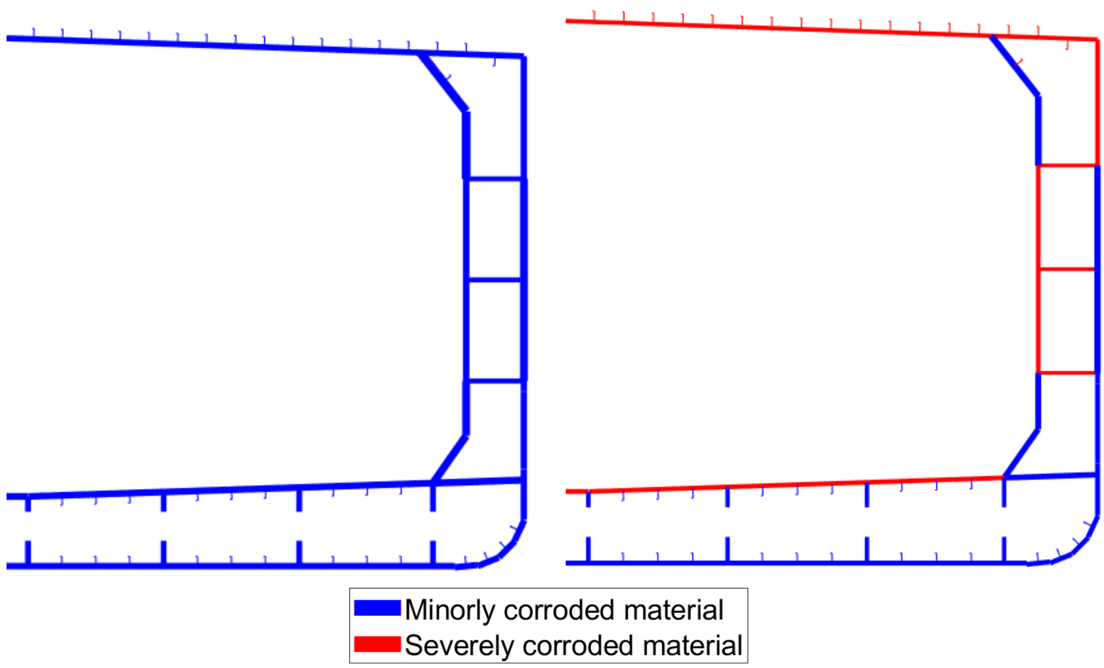

Figure 3.4 (left) 16-year-old tanker with corrosion material modeling considered; (right) 25-year-old tanker with corrosion material modeling considered.

3.3.3 Residual strength

The reduction in the hull girder longitudinal strength can be assessed by comparing the ultimate bending moments found for each corroded or damaged tanker with those calculated for the as-built undamaged tanker. The difference is quantified with the residual strength index (*RSI*), a concept first introduced by Fang and Das (2004). The *RSI* is the ratio of the ultimate bending moment of the damaged hull to the ultimate bending moment of the as-built hull, for a given loading condition. This is shown in Equation (3.6)

$$RSI = \frac{M_{U,damaged}}{M_{as\_built}} \tag{3.6}$$

where the ultimate bending moment found for the new and undamaged hull structure is used as M_{as_built}, and $M_{U,damaged}$ is the ultimate bending moment of all other ship conditions, including the intact corroded ones.

According to the definition of *RSI*, unless fully plastic bending moment is of concern, the following condition should be satisfied:

$$0 \leq RSI \leq 1 \qquad (3.7)$$

where the *RSI* value indicates the percentage of remaining longitudinal bending strength.

4 Results and discussion

The findings from the FE grounding simulations are discussed in Section 4.1. This is followed by a discussion of the ULS analyses in Section 4.2. The grounding and ULS results presented in this chapter reveal the effect that vessel age has on its resistance to hull penetration from grounding events and on its ultimate hull girder strength. They also show the importance of considering the altered material properties of corroded steel, opposed to just reducing the thicknesses.

4.1 FE grounding simulations

As explained in Section 3.2, the relevant results from the FE grounding simulations are the failure mode, damage size and shape, reaction forces on the rock, and internal and friction energies. Errors arising from modeling methods are first addressed in Section 4.1.1. Reaction forces and failure modes are discussed for selected cases in Section 4.1.2. With an emphasis on the effects of corrosion, the results are compared in Section 4.1.3.

4.1.1 Simulation errors

It is observed in several of the simulations that there are errors in the recorded force reactions during the transitions from the penetration to horizontal step and from the horizontal to removal step. The simulation with the largest errors is case T-C100-2; see Figure 4.1. This is therefore the simulation that is used to investigate the source of the errors.

It is assumed that the errors could arise due to the rock's sudden change in velocity; the rock's speed is 5 knots in all three steps, but with 45^o entrance and exit angles the sudden changes in the horizontal and vertical velocity components are significant. The entrance and exit angles were reduced to 20^o to test this hypothesis. To ensure that the horizontal step starts at the same longitudinal position, the rock was moved backwards prior to starting the simulation; all other settings were consistent with those described in Section 3.2. In Figure 4.2 it is observed that the error in the longitudinal reaction force at the transition between entrance and horizontal steps is not present with the shallower entrance angle.

Since the relevant results for this study are those recorded during the horizontal step, the spikes are not problematic if they do not affect the force reactions and resulting damage for the horizontal step. The longitudinal force reactions for the two simulations are compared in Figure 4.3. The average longitudinal reaction forces for the simulations with the 45^o and 20^o entrance angles are 3.59 MN and 3.56 MN, respectively, which is only a difference of 0.84%. Therefore, it is determined that the results are valid despite the errors.

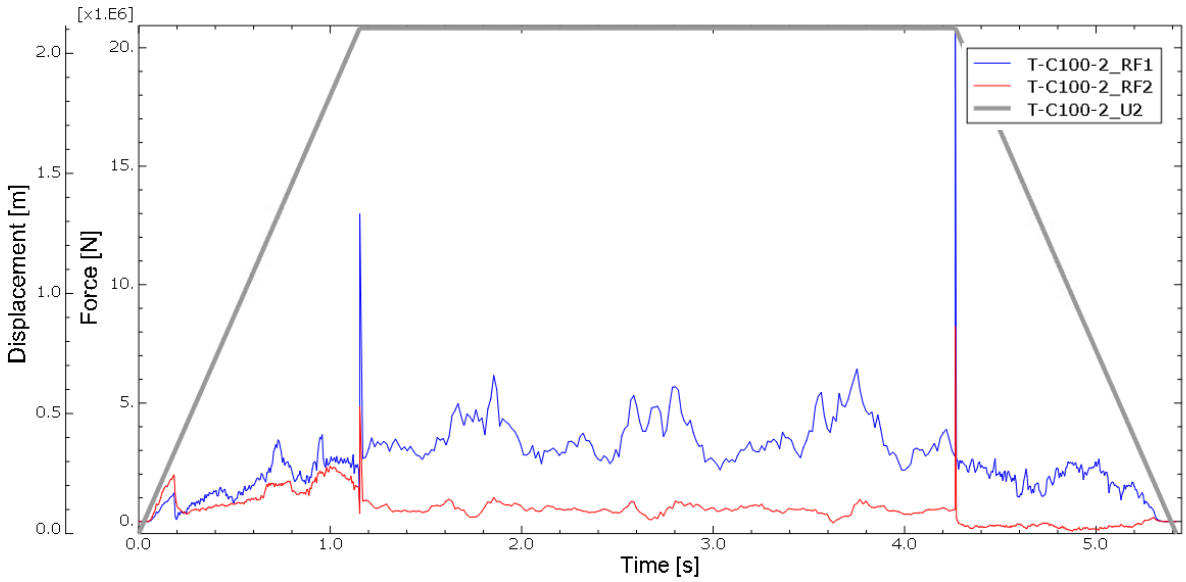

Figure 4.1 Force reactions on the rock for case T-C100-2; RF1 and RF2 are the reaction forces in the longitudinal and vertical directions, respectively and U2 is the vertical position of the rock.

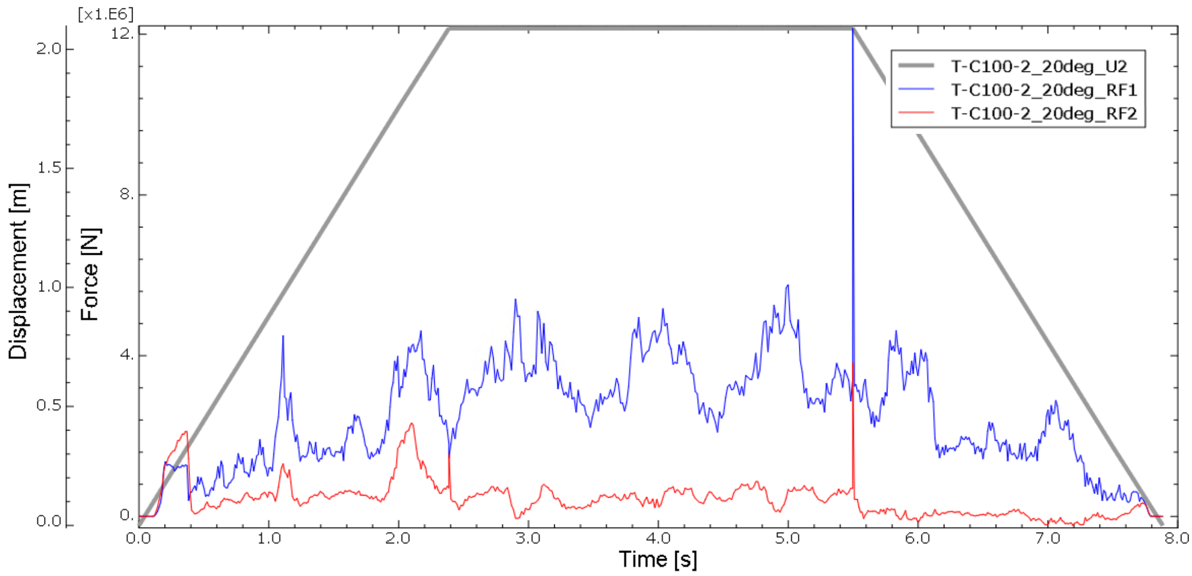

Figure 4.2 Force reactions on the rock for case T-C100-2 with the penetration and removal angles changed from 45º to 20º with respect to the BL; RF1 and RF2 are the reaction forces in the longitudinal and vertical directions, respectively and U2 is the vertical position of the rock.

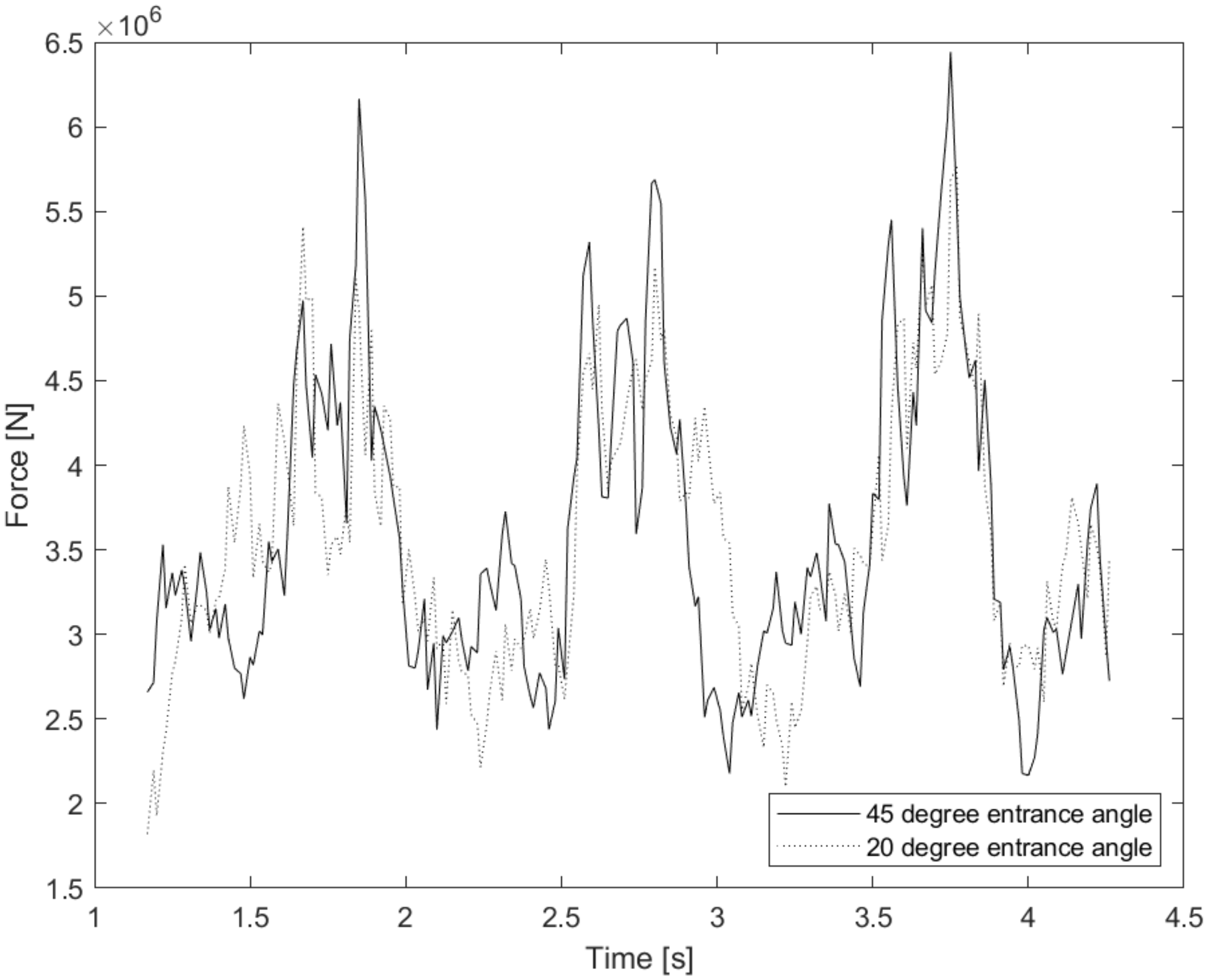

Figure 4.3 Longitudinal force reaction on the rock during the horizontal step for case T-C100-2 and for the same case with a modified entrance angle.

4.1.2 Damage openings from select cases

Figure 4.4 shows the damage to the double bottom of the 25-year-old tanker when it is grounded on the narrow rock. These results show that the damage opening is similar, regardless of the penetration location and the material model used. In all four cases, the predominant failure mode is local tearing. Global structural deformation is not seen, and the damage opening is confined between longitudinal girders. The same observations are made from the simulations with the zero and 25-year-old tankers. It is shown in Section 4.1.3 that the longitudinal reaction forces vary between these cases, but the resulting damage length is still the same since the rock's path was determined before the simulation.

The damage to the double bottom of the 25-year-old tanker after grounding on the wide rock is shown in Figure 4.5. Unlike the simulations with the narrow rock, the ones with the wide rock leave the inner bottom plating deformed, but intact. Additionally, the groundings with the wide rock result in different failure modes and damage openings depending on the material model used. Local crushing of frames and longitudinal girders is seen during the grounding incidents, regardless of the material model; however, significant global deformation is only observed with the cases wherein the tanker was modeled with the non-corroded constitutive material model. Moreover, the damage opening is smaller for the cases with the non-corroded material model. The local tearing that is observed with the narrow rock and the crushing that is seen with the wide rock are consistent with the failure modes observed with similar ground shapes in the grounding study done by Alsos and Amdahl (2007). The size and shape of the damage opening is significant since this affects the damage stability, longitudinal strength of the tanker, and eventual oil spill.

Figure 4.6 show the resulting cross-sectional areas of the longitudinal members for all 20 grounding simulations. In general, the areas reduce as the tanker's age increases; this is expected since the CMs are reduced linearly over time. It is seen that the resulting areas after grounding damage from the narrow rock are similar, regardless of the material model used. And it is confirmed by observations in Figure 4.4 that the damage openings are similar for these cases. However, if the areas that result after groundings on the wide rock are compared, it is observed that for both the 16 and 25-year-old tankers, the areas are larger if the non-corroded constitutive material model is used, reaffirmed by the results shown in Figure 4.5.

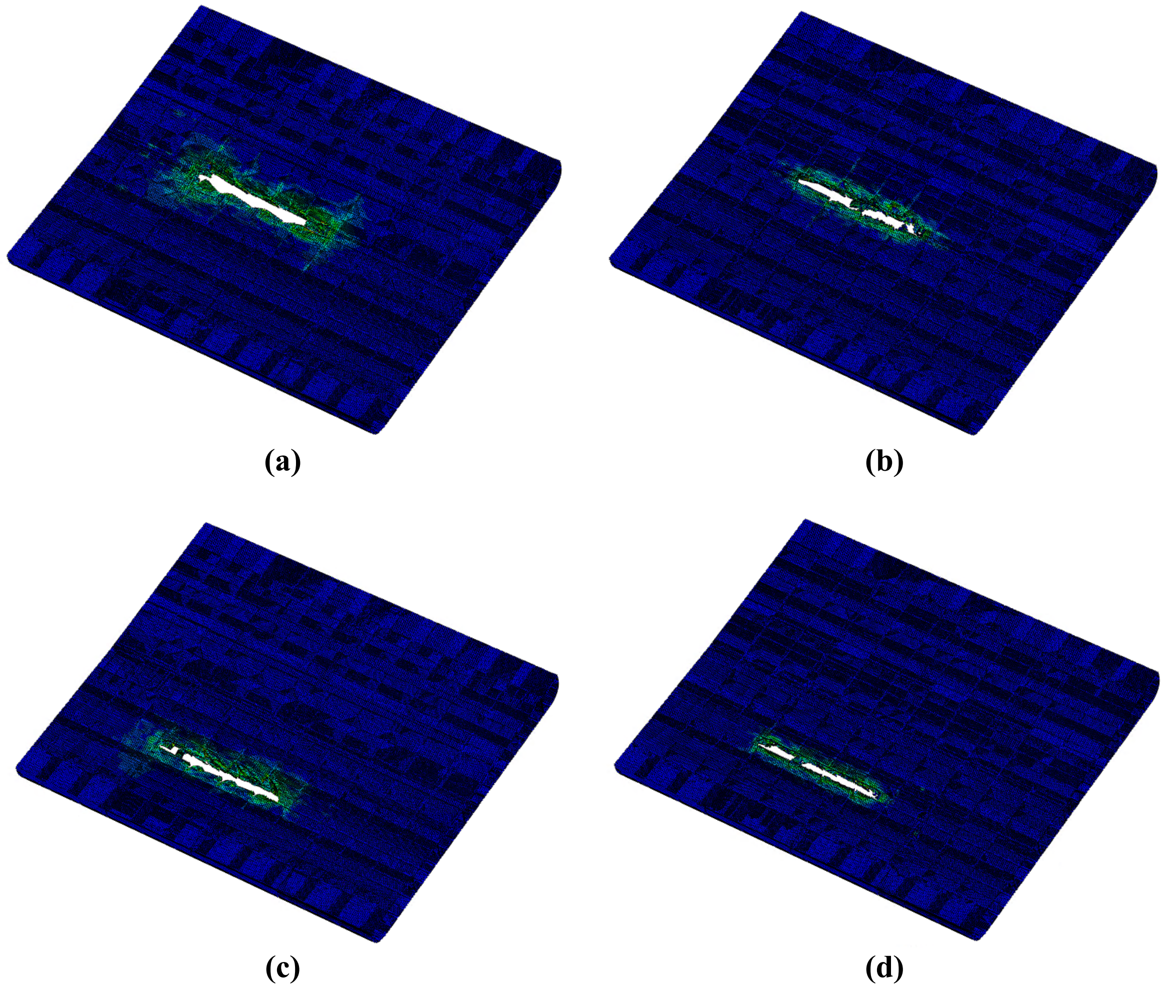

*Figure 4.4 Resulting bottom damage on the 25-year-old tanker from the narrow rock; **(a)** CL, 100% CM reduction, and non-corroded material model (i.e. case T-C100-5); **(b)** CL, 100% CM reduction, and minorly and severely corroded material models (i.e. case T-C100-1); **(c)** 1/4B, 100% CM reduction, and non-corroded material model (i.e. case T-C100-6); **(d)** 1/4B, 100% CM reduction, and minorly and severely corroded material models (i.e. case T-C100-2).*

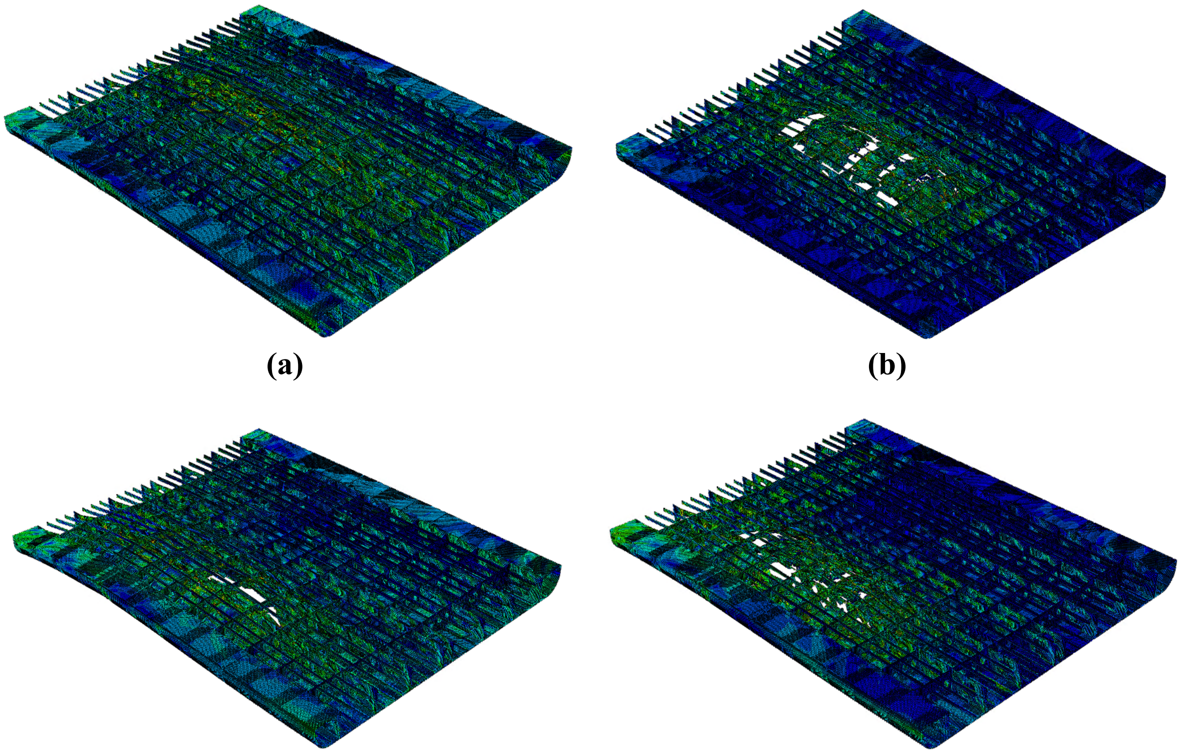

(a) **(b)** **(c)** **(d)**

Figure 4.5 Resulting bottom damage on the 25-year-old tanker from the wide rock; ***(a)*** *CL, 100% CM reduction, and non-corroded material model (i.e. case T-C100-7);* ***(b)*** *CL, 100% CM reduction, and minorly and severely corroded material models (i.e. case T-C100-3);* ***(c)*** *1/4B, 100% CM reduction, and non-corroded material model (i.e. case T-C100-8);* ***(d)*** *1/4B, 100% CM reduction, and minorly and severely corroded material models (i.e. case T-C100-4).*

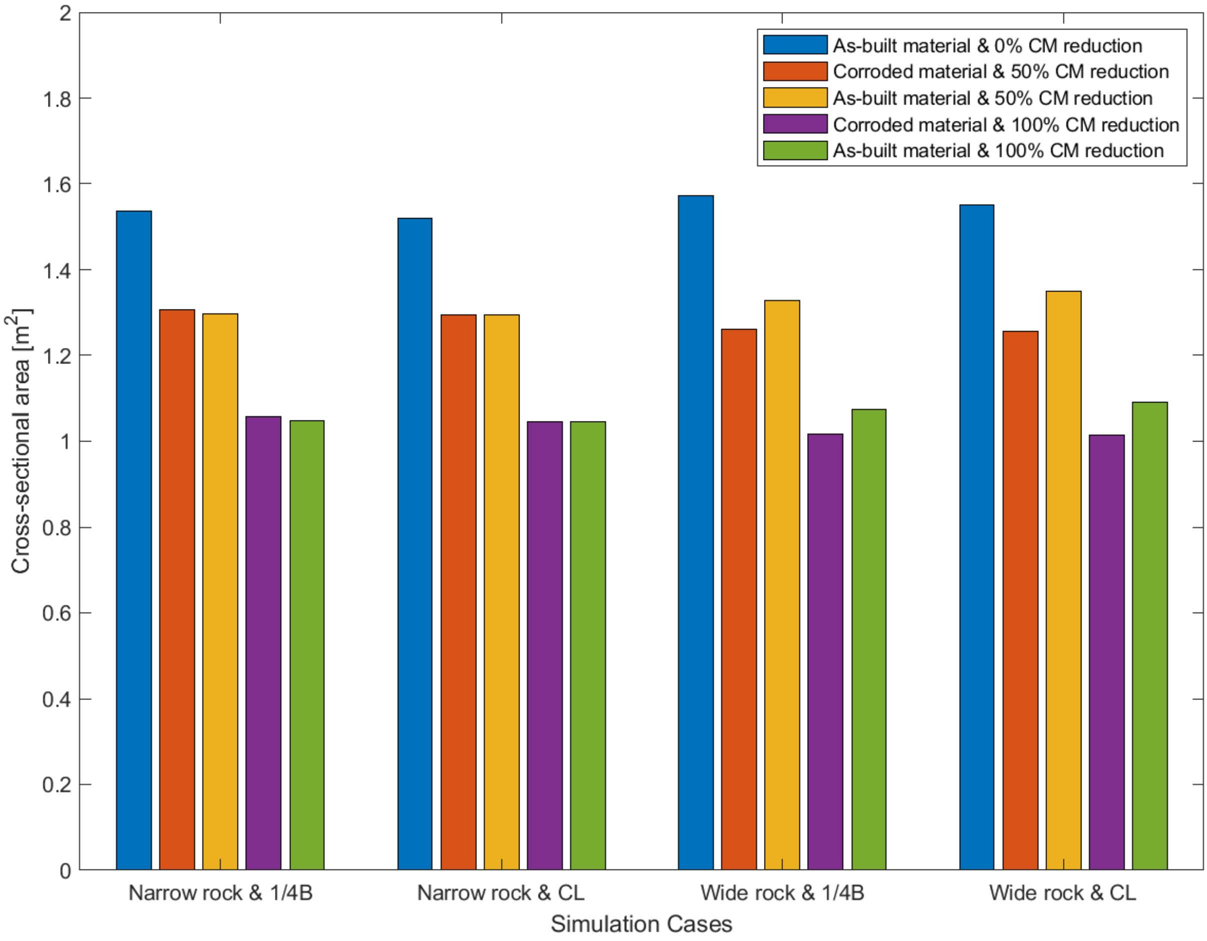

Figure 4.6 Net cross-sectional areas of longitudinal members at the cross-section used for the bending simulations.

4.1.3 Conclusions from grounding cases

In order to make conclusions on the effects of corrosion and corrosion modeling on grounding damage predictions, the following sets of grounding cases are compared:

1. T-AB-1, T-C50-1, T-C50-5, T-C100-1, and T-C100-5
2. T-AB-2, T-C50-2, T-C50-6, T-C100-2, and T-C100-6
3. T-AB-3, T-C50-3, T-C50-7, T-C100-3, and T-C100-7
4. T-AB-4, T-C50-4, T-C50-8, T-C100-4, and T-C100-8

Comparisons one and two consist of all the cases with the narrow rock, and the third and fourth comparisons consist of all the cases with the wide rock. See Section 3.1 for a complete description of each simulation case. Figures 4.7 through 4.10 show the longitudinal reaction forces for comparisons one through four, respectively. The average longitudinal reaction forces that were recorded during the horizontal step are shown for all simulation cases in Figure 4.11.

It is observed that for the narrow rock, reducing the CM without changing the constitutive material model results in reduced longitudinal reaction forces. For the first comparison, i.e. when the narrow rock penetrates the double bottom on the hull's CL, the average longitudinal reaction forces are reduced by 5.5 and 31.9 percent for CM reductions of 50 and 100 percent, respectively, when compared with the average longitudinal reaction force for case T-AB-1. Similarly, for comparison two, i.e. when the narrow rock penetrates the hull at 1/4B, the average longitudinal reaction forces are reduced by 4.3 and 28.0 percent for CM reductions of 50 and 100 percent, respectively, when compared to the average longitudinal reaction force from case T-AB-2.

However, when both thicknesses and material models are changed for aged hull structures, the average longitudinal reaction force is reduced significantly more. For the first comparison, the average longitudinal reaction forces are reduced by 55.5 and 66.8 percent for cases T-C50-1 and T-C100-1, respectively, when they are compared with the average longitudinal reaction force for case T-AB-1. For comparison two, when the narrow rock penetrates the hull at 1/4B, the average longitudinal reaction forces are reduced by 52.5 and 65.7 percent for cases T-C50-2 and T-C100-2, respectively, when these forces are compared to those recorded for case T-AB-2. This is significant since it means that the dissipated frictional and internal energies for a given damage length are overestimated by about 100 percent for both the 16 and 25-year-old tankers, when only the CM reduction is considered. This means that the damage length is underestimated by 50 percent for both the 16 and 25-year-old tankers if the material properties of aged ships are not considered.

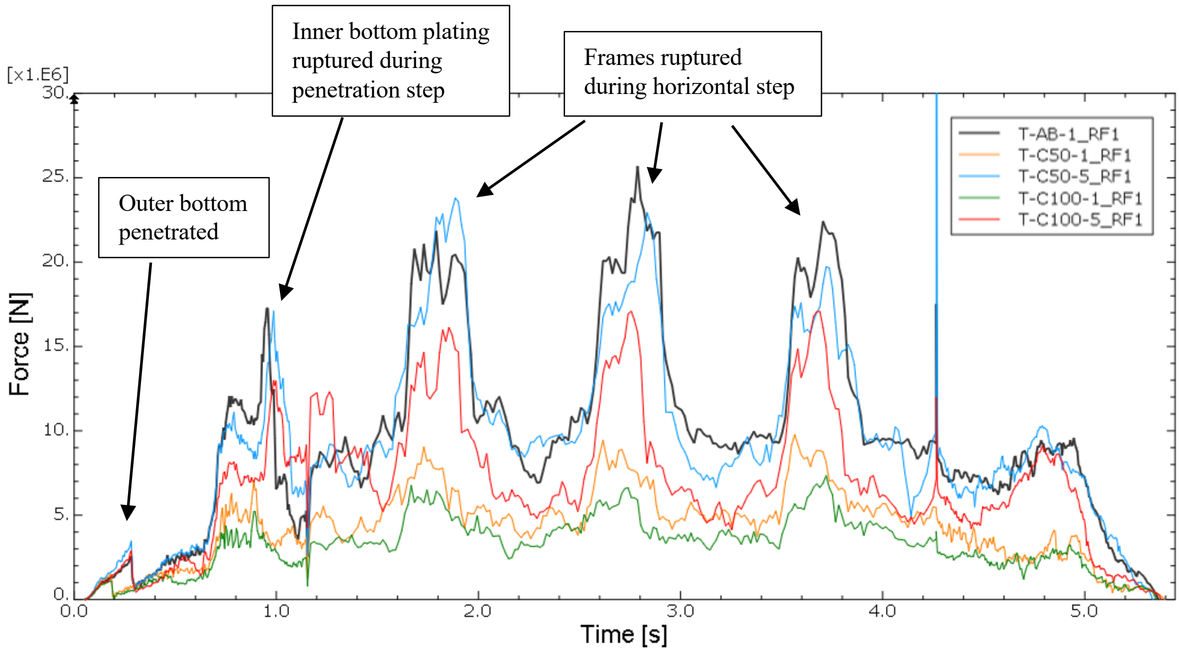

Figure 4.7 Comparison of horizontal reaction forces for cases T-AB-1, T-C50-1, T-C50-5, T-C100-1, and T-C100-5.

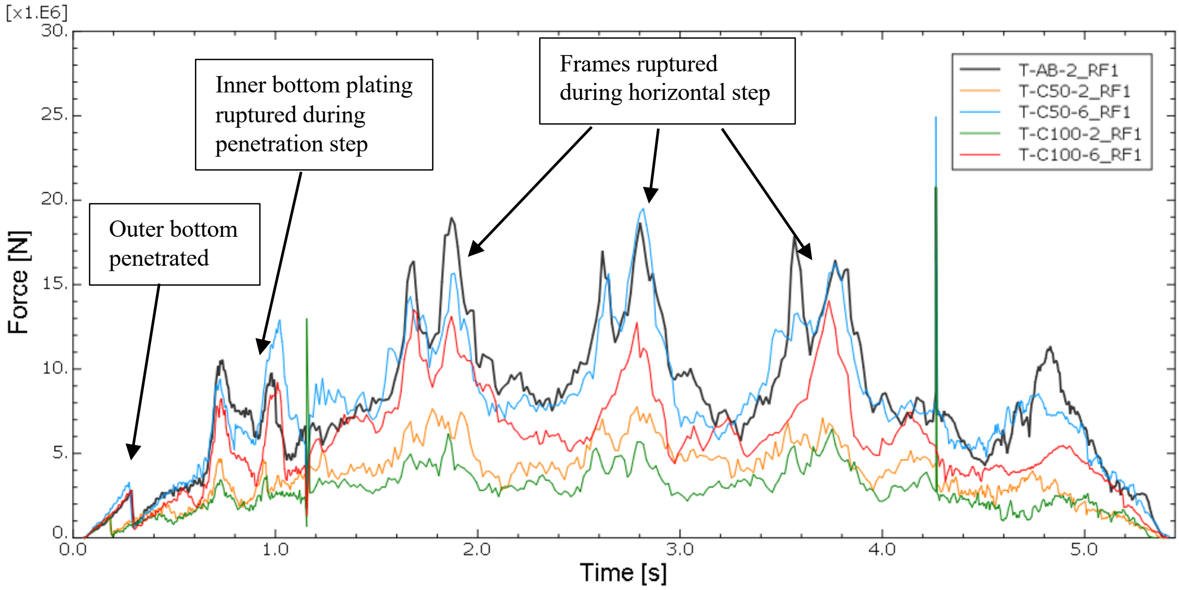

Figure 4.8 Comparison of horizontal reaction forces for cases T-AB-2, T-C50-2, T-C50-6, T-C100-2, and T-C100-6.

For the wide rock, the simulation results indicate that the longitudinal reaction force is, in most cases, increased if the CM is reduced without changing the material properties; this phenomenon is possibly a result of the reduced rigidity of the hull girder, i.e. the hull girder is able to withstand more deflection before material rupture ensues. However, if the CM is reduced and the material properties are changed to match those of corroded steel, then the longitudinal reaction force reduces as the hull structure ages. For the wide rock, it is seen that the reduction in reaction force is approximately the same from zero to 16 years as it is from 16 to 25 years.

For the third comparison, i.e. when the wide rock penetrates the hull on its CL, the average longitudinal reaction forces are increased by 27.0 and 1.1 percent for cases T-C50-7 and T-C100-7, respectively, when compared to the average longitudinal reaction force for case T-AB-3. However, for cases T-C50-3 and T-C100-3, the average longitudinal reaction forces are reduced by 20.3 and 38.9 percent, respectively. Since the dissipated energy is approximated as the average longitudinal reaction force times the longitudinal distance the rock moves during the horizontal step, that means that the dissipated energies are overestimated by 59 and 65 percent for the 16 and 25-year-old tanker, respectively, when the wide rock penetrates the hull on its CL and the constitutive material model is not changed to represent the properties of corroded steel. Therefore, the damage length would be underestimated by 37 and 39 percent for the 16 and 25-year-old tanker, respectively, if thicknesses are reduced without also changing the constitutive material model.

For the fourth comparison, i.e. for the cases when the wide rock penetrates the double bottom at 1/4 B, the average longitudinal reaction force is increased by 18.7 percent for the 16-year-old tanker and decreased by 4.5 percent for the 25-year-old tanker when only thicknesses are reduced. However, when both CMs are reduced and constitutive material models are changed, the average longitudinal reaction forces are reduced by 11.6 and 30.8 percent for the 16 and 25-year-old tankers, respectively. These differences indicate that the damage length would be underestimated by 25 and 28 percent for the 16 and 25-year-old tankers, respectively, if the constitutive material model is not changed.

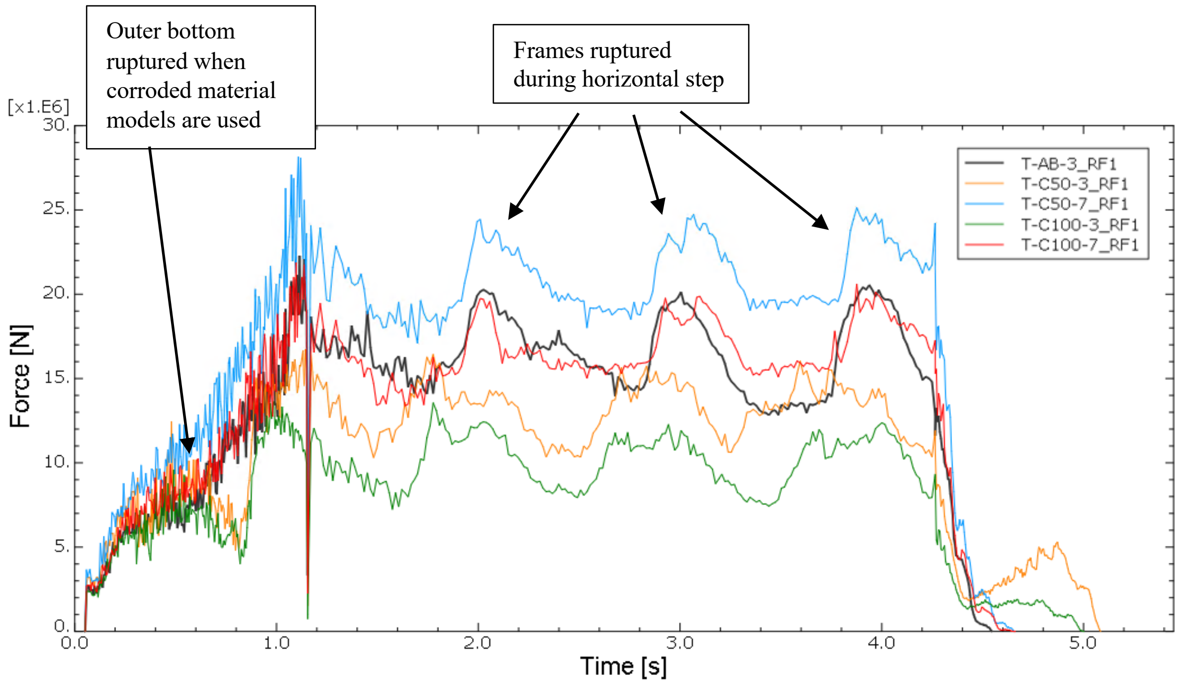

Figure 4.9 Comparison of horizontal reaction forces for cases T-AB-3, T-C50-3, T-C50-7, T-C100-3, and T-C100-7.

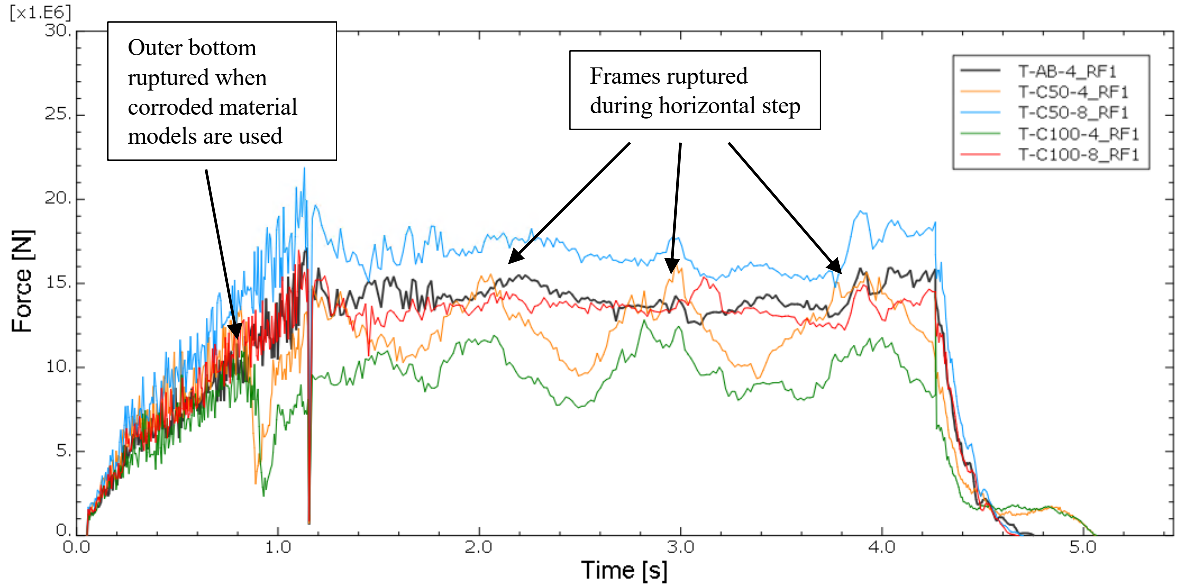

Figure 4.10 Comparison of horizontal reaction forces for cases T-AB-4, T-C50-4, T-C50-8, T-C100-4, and T-C100-8.

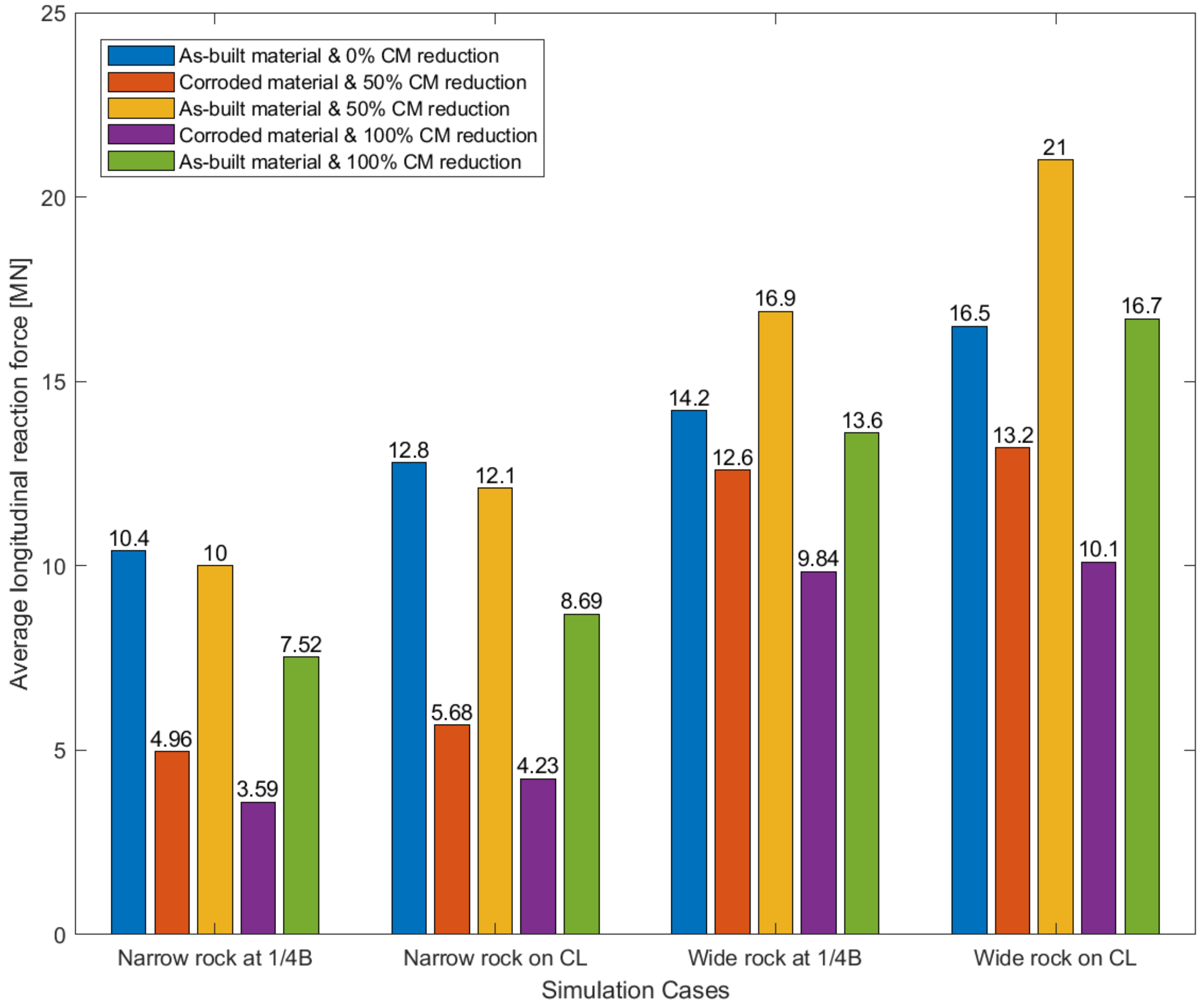

Figure 4.11 Average longitudinal reaction forces during the horizontal step.

Figure 4.11 shows that the average longitudinal reaction forces are higher for the wide rock than they are for the narrow rock. The figure also shows that the reaction forces are higher when the hull bottom is penetrated on the vessel's CL, regardless of the rock geometry. Therefore, the damage length would be the longest if the hull were to be penetrated at 1/4B with the narrow rock; it would be the shortest with the wide rock on the tanker's CL. The longitudinal reaction forces for the 20 simulations indicate that it is necessary to consider the altered material properties when assessing the crashworthiness of aged vessels, regardless of the rock geometry and the penetration location. If the constitutive material model is not representative of the actual condition of the steel of an aged hull, the reaction forces and the associated dissipated energy would be overestimated, resulting in shorter damage opening due to grounding. This would result in the misconception that the vessel is more crashworthy than it is.

4.2 Ultimate limit state analyses

The resulting ultimate bending moments that were determined for each condition of the tanker are discussed in Section 4.2.1. Section 4.2.2 follows with an interpretation of the various ultimate limit states, using the *RSI*. T-AB is the as-built intact tanker, and it is used as the reference case throughout the analysis. For the other intact cases, namely T-16tm, T-16t, T-25tm, and T-25t, the letters t and m indicate that the thicknesses were reduced and that the material properties were changed, respectively; the numbers 16 and 25 correspond with the vessel's age, and thus indicate the CM reduction percentage and the material properties. For the damaged cases, the tanker IDs correspond with the geometries that result from their respective simulation cases in Table 3.1. The damaged models that were used in the ULS analyses are shown in Appendix A.

4.2.1 Ultimate bending moments in intact conditions

Figure 4.12 shows the ultimate bending moments found for the loading conditions applied to the five different intact tanker models. For each tanker model, its ultimate bending moment occurs in the purely horizontal bending condition. This is expected since its beam is greater than its depth. For the purely vertical bending condition, i.e. 90° and 270°, the tanker, at all stages of its service life, is more resistant to failure in hogging than in sagging. This is also expected since the tanker has a double bottom that results in the initial horizontal NA being closer to the outer bottom than to the weather deck. Thus, for a given curvature, the stresses are smaller in the outer bottom compared to the weather deck. Additionally, due to the increased stiffness of the double bottom, the tanker's ULS is higher in hogging than in sagging because yielding of the weather deck may precede buckling of the double bottom.

It is observed in Figure 4.12 that the ultimate bending moment decreases linearly from the start to the end of its service life. This is not surprising since the CMs were reduced linearly. Changing the material properties to match those of the minorly and severely corroded materials reduces the tankers bending ULS further; however, only a small difference is seen.

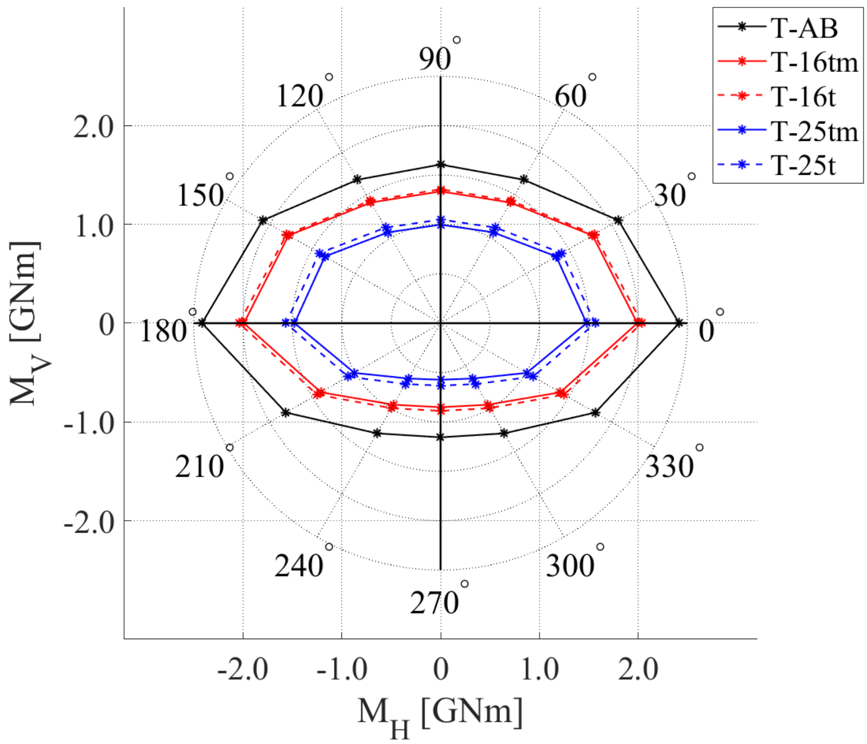

Figure 4.12 Biaxial bending under prescribed bending control for all conditions of the intact tanker.

Similar results are observed for the tankers with bottom damage, in that the general shape of the curves remains. For the tankers with damage on the CL, the ultimate bending moments remain almost the same when subjected to sagging and horizontal bending moment loads;

however, the ultimate bending moments in hogging are significantly reduced. For the models with damage on the starboard side, the same observation holds, with the exception that the ultimate bending moment is reduced when the starboard side is in compression. These results are reasonable since the NA is shifted away from the damaged area.

4.2.2 Reduced ultimate bending moment

Figure 4.13 shows the *RSI* values for all ages of the intact tanker. It is observed that, regardless of the method used to model corrosion related deterioration, the ULS is decreased the most for the sagging condition, and the least for the hogging condition. The *RSI* values for hogging and sagging conditions are shown in Table 4.1. It is seen that the material properties only have a small effect on the reduction of the tanker's longitudinal strength, i.e. most of the reduction is due to the reduced CM.

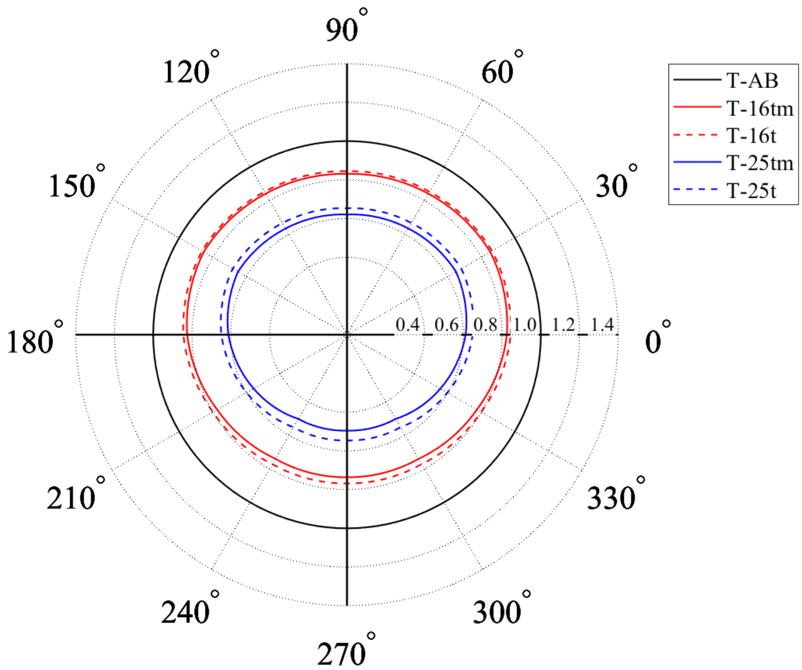

Figure 4.13 RSI polar plot for all conditions of the intact tanker.

Table 4.1 RSI values for the 16 and 25-year-old tankers in their intact conditions; values taken from Figure 4.13.

	T-16tm	T-16t	T-25tm	T-25t
Hogging	0.831	0.845	0.621	0.653
Sagging	0.736	0.768	0.495	0.547

The *RSI* values for all damaged cases are shown in Figure 4.14. For all cases, the ultimate bending moments obtained for T-AB are used to nondimensionalize the results. It is seen in Figures 4.14 **(a)** and 4.14 **(b)** that there is only a small difference in the ULS when the material model is changed to correspond with the level of corrosion. Most of the reduction in longitudinal strength comes from the reduction in thickness. This makes sense since the narrow rock caused similar damage to all models, regardless of their age, and since it was shown in Figure 4.13 that the reduced CM was predominantly responsible for the reduced longitudinal strength. However, in Figures 4.14 **(c)** and 4.14 **(d)** it is seen that reducing the CMs and changing the material properties have roughly the same impact on the ship's ULS reduction.

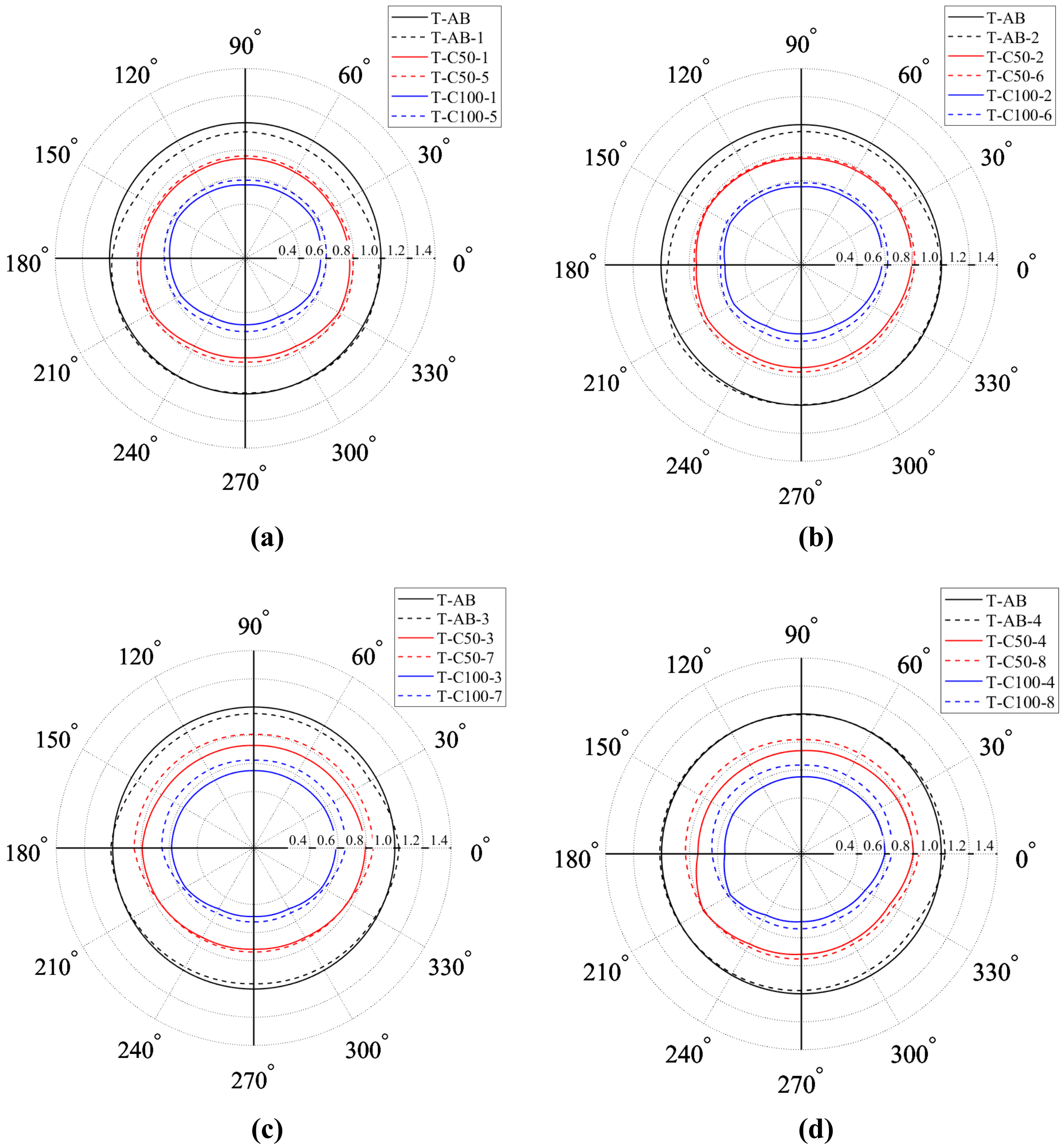

Figure 4.14 RSI polar plots for all cases with ***(a)*** *narrow rock penetrating at CL,* ***(b)*** *narrow rock penetrating at B/4,* ***(c)*** *wide rock penetrating at CL, and* ***(d)*** *wide rock penetrating at B/4.*

The grounding simulations with the narrow rock resulted in almost the same amount of damage, regardless of the material model and the CM reduction; see Figures 4.4 and 4.6. However, for the grounding simulations with the wide rock, there was a significant difference in the damage caused to the bottom structure when different material models were used; see Figures 4.5 and 4.6. It was found that for the aged tankers with the as-built NVA material model, the double bottom was not fully penetrated by the wide rock; rather, the structure's increased yield and ultimate strengths resulted in increased vertical deflection of the inner bottom and supporting structural members. Furthermore, this deflection was not confined to the width of the rock. On the contrary, for the tankers with the minorly and severely corroded material models, the damage openings were fully developed, and the vertical deflection of the inner bottom was confined to the width of the rock. While Figures 4.14 **(c)** and 4.14 **(d)** indicate that changing the material model has a significant effect on the ULS reduction, in light of the observations from Figures 4.6, 4.13, 4.14 **(a)**, and 4.14 **(b)**, it is likely that it is the resulting geometry and the net cross-sectional area of the longitudinal structural members, not the material properties, that are predominantly responsible for the reduced bending ULS. However, the constitutive material model used in the grounding simulations directly affected the resulting geometry and net cross-sectional area of the longitudinal structural members. The constitutive material model thus indirectly affects the ULS of the damaged tanker.

4.2.3 Conclusions from ULS analyses

Although the material properties only have a small effect on the calculated biaxial bending ULS when using the Smith method that was further developed by Fujikubo et al. (2012), the geometry and the cross-sectional area of the cross section has a significant effect. It is therefore important to use realistic hull models that are representative of the actual damage. As discussed in Section 4.1.3, the only way to obtain results with realistic damage is to use a constitutive material model that is representative of the condition of the steel. When determining the ULS of damaged ship structures, it is therefore important to use hull models that resulted from grounding simulations wherein representative constitutive material models were used. With the modified Smith method, the material properties affect the results to some degree, but it is more important to use an accurate and representative hull geometry.

5 Conclusions

The effects of corrosion on the grounding resistance and failure modes were investigated by using double bottom hull structures that had been in service for zero, 16, and 25 years. Their material degradation was considered with two different approaches in order to determine the importance of accounting for the altered material properties caused by corrosion. The first, and most commonly used method, was to reduce the CM without changing the constitutive material model from that of the as-built tanker. The second method was to reduce the CM by the same amount and to also change the constitutive material model. It was found that grounding damage is underestimated by up to 50 percent if the constitutive material model is not changed for corroded steel. The results showed that the narrow rock results in similar damage patterns, regardless of the constitutive material model; however, the extent of the damage opening caused by the wide rock is dependent on the constitutive material model. This study thus corroborates the results obtained by Kuznecovs and Shafieisabet (2017), wherein the importance of changing the material constitutive model for ship-ship collisions was shown.

Using the URSA code, the Smith method, as modified by Fujikubo et al. (2012) was then used to determine the ULS of the intact and damaged tanker models when subjected to different horizontal and vertical moment combinations. Cross-sections of the tanker's hull girder were built up by integrating the damaged double bottom structure from each grounding case with the tanker's sides and weather deck. It was observed that the material properties have a minor effect on the biaxial bending ULS; the most significant factor is the cross-sectional area of the longitudinal structural members in the cross-section that is used in the biaxial bending analyses.

In the grounding simulations, it was revealed that the constitutive material model significantly affects the shape and size of the damage opening, and thus the resulting cross-sectional area. Additionally, the ULS analyses revealed a strong inverse relationship between the cross-sectional area of the tanker's hull girder and the ultimate bending moment. Thus, the results of the grounding simulations and the ULS analyses revealed the importance of using a constitutive material model that is representative of the current condition of the vessel, when running the grounding simulations.

The results of this study indicate that reducing the thicknesses alone, results in overestimations of the vessel's crashworthiness and residual strength. To ensure that a vessel's safety is sufficient at the end of its service life, it could be necessary to use a reduced yield strength and material stiffness when implementing classification societies' structural calculations.

6 Future work

The subject of ship groundings, corrosion, and ULS analyses have been studied for a long time, but there are still many topics that require further investigation for better understanding. The following topics are considered relevant and thus warrant further investigation:

- Verify the results obtained with the larger rock by using a longer model wherein large stresses do not extend to the BCs.
- Continue investigating different rock entrance angles to determine what is required to eliminate force spikes between simulation steps.
- Verify the methods used for the grounding simulations by creating an FE model of the hull structure used in the experiments done by Rodd (1997) at the Naval Surface Warfare Center.
- Perform the same parametric study, but with the modification of using one of the coupled methods for the grounding simulations. This would generate more realistic bottom damages that could be used in a ULS investigation. It would be interesting to see how significantly those ULS results vary from the ones obtained in this study.
- Perform the same study but with the addition of including the welding induced residual stresses in the FE model.
- Include the centerline longitudinal bulkhead to see if the results obtained by Heinvee et al. (2016) can be corroborated.
- It would be interesting to verify the method used in this study for the estimation of the material properties of corroded steel. This could be done by performing tensile tests with tensile test specimens made with NVA shipbuilding steel that have varying degrees of corrosion. It would be interesting to see if the results of such an experiment would yield similar material properties as those predicted with the method used in this study.
- The ULS investigation in this study should be continued by performing nonlinear FEA bending simulations. It would be interesting to use models with varying extents of bottom damage to verify that the calibrated Smith method that was proposed by Kuznecovs et al. (2020) can be used to accurately predict the bending ULS of hull girders with bottom damage.
- It is common to use friction coefficients of 0.3 and 0.5 for non-corroded and corroded steel hulls, respectively. Sensitivity studies have been done to investigate the influence of friction coefficients, but different studies have yielded contradictory results. Thus, it could be worthwhile to investigate this further for different grounding scenarios.

References

AbuBakar, A. and Dow, R.S. (2013). *Simulation of ship grounding damage using the finite element method*. International Journal of Solids and Structures, 50(1): 623-636.

Alianz Global Corporate & Specialty. (2019). *Safety and shipping review 2019*.

Alsos, H.S. and Amdahl, J. (2007). *On the resistance of tanker bottom structures during stranding*. Marine Structures*,* 20, 218-237.

Dassault Systèmes (2020). *Abaqus unified FEA*. Available online [accessed: 2020-05-20]: https://www.3ds.com/products-services/simulia/products/abaqus/.

Fang, C. and Das, P.K. (2004). *Hull girder ultimate strength of damaged ships*. In: Proceedings of the 9th Symposium on Practical Design of Ships and Other Floating Structures (PRADS 2004), Lübeck-Travemuende, Germany, 309-316.

Fujikubo, M., Takemura, K., Oka, S., Alie, M.Z.M., and Iijima, K. (2012). *Residual hull girder strength of asymmetrically damaged ships*. Journal of the Japan Society of Naval Architects and Ocean Engineers, 16(1): 131-140.

Garbatov, Y., Soares, G. C., Parunov, J., and Kodvanj, J. (2014). *Tensile strength assessment of corroded small scale specimens*. Corrosion Science*,* August, 85, 296-303.

Heinvee, M. and Tabri, K. (2015). *A simplified method to predict grounding damage of double bottom tankers*. Marine Structures*,* 43, 22-43.

Heinvee, M., Tabri, K., Korgesaar, M., and Urbel, A. (2016). *Influence of longitudinal and transverse bulkheads on ship grounding resistance and damage size*. In: The 7th International Conference on Collision and Grounding of Ships (ICCGS), Ulsan, South Korea 15-18 Jun. 2016.

Hogström, P. (2012). *RoPax Ship Collision - a Methodology for Survivability Analysis,* Licentiate Thesis. Chalmers University of Technology, Gothenburg, Sweden: Chalmers Reproservice.

Hogström, P., Ringsberg, J.W., and Johnson, E. (2009). *An experimental and numerical study of the effects of length scale and strain state on the necking and fracture behaviours in sheet metals*. International Journal of Impact Engineering, 36(10-11), 1194-1203.

Hogström, P. and Ringsberg, J. W. (2011). *An extensive study of a ship's survivability after collision – a parameter study of material characteristics, nonlinear FEA and damage stability analyses.* Marine Structures.

Hooper, J.J., Foecke, T., Graham, L., and Weihs, T.P. (2003). *Metallurgical Analysis of Wrought Iron From the RMS Titanic*. Marine technology*,* 40, 73-81.

International Association of Classification Societies (IACS). (2020). *Common Structural Rules for Bulk Carriers and Oil Tankers*. Available online [accessed: 2020-05-20]: http://www.iacs.org.uk/publications/common-structuralrules/csr-for-bulk-carriers-and-oil-tankers/.

International Maritime Organization (IMO). (2020). *History of SOLAS (The International Convention for the Safety of Life at Sea)*. Available online [accessed: 2020-02-15]: http://www.imo.org/en/KnowledgeCentre/ReferencesAndArchives/HistoryofSOLAS/Pages/default.aspx.

International Maritime Organization (IMO). (2010). *Resolution MSC.287 - Adoption of the International Goal-Based Ship Construction Standards for Bulk Carriers and Oil Tankers*. Available online [accessed: 2020-05-20]: http://www.imo.org.

Kuznecovs, A., Ringsberg, J.W., Johnson, E., and Yamada, Y. (2020). *Ultimate limit state analysis of a double-hull tanker subjected to biaxial bending in intact and collision-damaged conditions*. Submitted for publication in Ocean Engineering (under review).

Kuznecovs, A. and Shafieisabet, R. (2017). *Analysis of the ultimate limit state of corroded ships after collision*. MSc thesis report X-17/376, Chalmers University of Technology, Gothenburg, Sweden.

Birkland, T.A. and Lawrence, R.G. (2002). *The Social and Political Meaning of the Exxon Valdez Oil Spill*. Spill Science & Technology Bulletin, 7, 17-22.

Liu, B., Pedersen, P.T., Zhu, L., and Zhang, S. (2018). *Review of experiments and calculation procedures for ship collision and grounding damage*. Marine Structures, 59, 105-121.

Liu, B. and Soares, G. (2016). *Review of experimental work on energy absorption in ship structural components*. In: The 7th International Conference on Collision and Grounding of Ships (ICCGS), Ulsan, South Korea 15-18 Jun. 2016.

Liu, B., Villavicencio, R., Zhang, S., and Soares, C.G. (2017). *Assessment of external dynamics and internal mechanics in ship collisions*. Ocean Engineering, 141, 326-336.

Mathworks Inc. (2019). *MATLAB R2019b Documentation.* Natick: Mathworks Inc.

Paik, J.K. (2018). *Ultimate limit state analysis and design of plated structures (2nd edition)*. Wiley-Blackwell, Hoboken, New Jersey, USA.

Paik, J. K., Lee, M. J., Sung, H. J., and Il, P. Y. (2003). *A Time-Dependent Corrosion Wastage Model for the Structures of Single- and Double-Hull Tankers and FSOs and FPSOs*. Marine Technology, 40(3), 201-217.

Parunov, J., Rudan, S., Gledić, I., and Primorac, B.B. (2018). *Finite element study of residual ultimate strength of a double hull oil tanker with simplified collision damage and subjected to bi-axial bending*. Ships and Offshore Structures, 13(S1): S25-S36.

Pedersen, P.T. and Zhang, S. (2000). *Absorbed energy in ship collisions and grounding – revising Minorsky's empirical method*. Journal of Ship Research, 44, 140-154.

Ringsberg, J.W., Li, Z., and Johnson, E. (2017). *Performance assessment of the crashworthiness of corroded ship hulls*. In: C.G. Soares and. Y. Garbatov (Eds.), Progress in the Analysis and Design of Marine Structures - Proceedings of the 6th International Conference on Marine Structures (MARSTRUCT 2017), Lisbon, Portugal. Taylor & Francis Group, London, UK, 523-531.

Ringsberg, J.W., Li, Z., Johnson, E., Kuznecovs, A., and Shafieisabet, R. (2018). *Reduction in ultimate strength capacity of corroded ships involved in collision accidents*. Ships and Offshore Structures, 13(S1): S155-S166.

Rodd, J.L. (1977). *Fame design effects in the rupture of oil tanks during grounding accidents*. In: The International Conference on Advances in Marine Structures III., 1997 Dera, Rosyth, UK.

Simonsen, B.C., Törnqvist, R., and Lützen, M. (2009). *A simplified grounding damage prediction method and its application in modern damage stability requirements*. Marine Structures, 22, 62-83.

Simonsen, B. C. (1997). *Ship Grounding on Rock - II. Validation and Application*. Marine Structures, 10, 563-584.

Smith, C.S. (1977). *Influence of local compressive failure on ultimate longitudinal strength of a ship's hull*. In: Proceedings of the 3rd International Symposium on Practical Design in Shipbuilding (PRADS 1977), Tokyo, Japan, 73-79.

Sormunen, O.E., Castren, A., Romanoff, J., and Kujala, P. (2016). *Estimating sea bottom shapes for grounding damage calculations*. Marine Structures, 45, 86-109.

Sun, B., Hu, Z., and Wang, J. (2017). *Bottom structural response prediction for ship-powered grounding over rock-type seabed obstructions*. Marine Structures, 54, 127-143.

Tekgoz, M., Garbatov, Y., and Soares, C.G. (2018). *Strength assessment of an intact and damaged container ship subjected to asymmetrical bending loadings*. Marine Structures, 58(1): 172-198.

Yu, Z. and Amdahl, J. (2016). *Influence of 6DOF ship motions in the damage prediction of ship collision and grounding accidents*. In: The 7th International Conference on Collision and Grounding of Ships (ICCGS), Ulsan, South Korea 15-18 Jun. 2016.

Appendix

A. Damaged tanker models

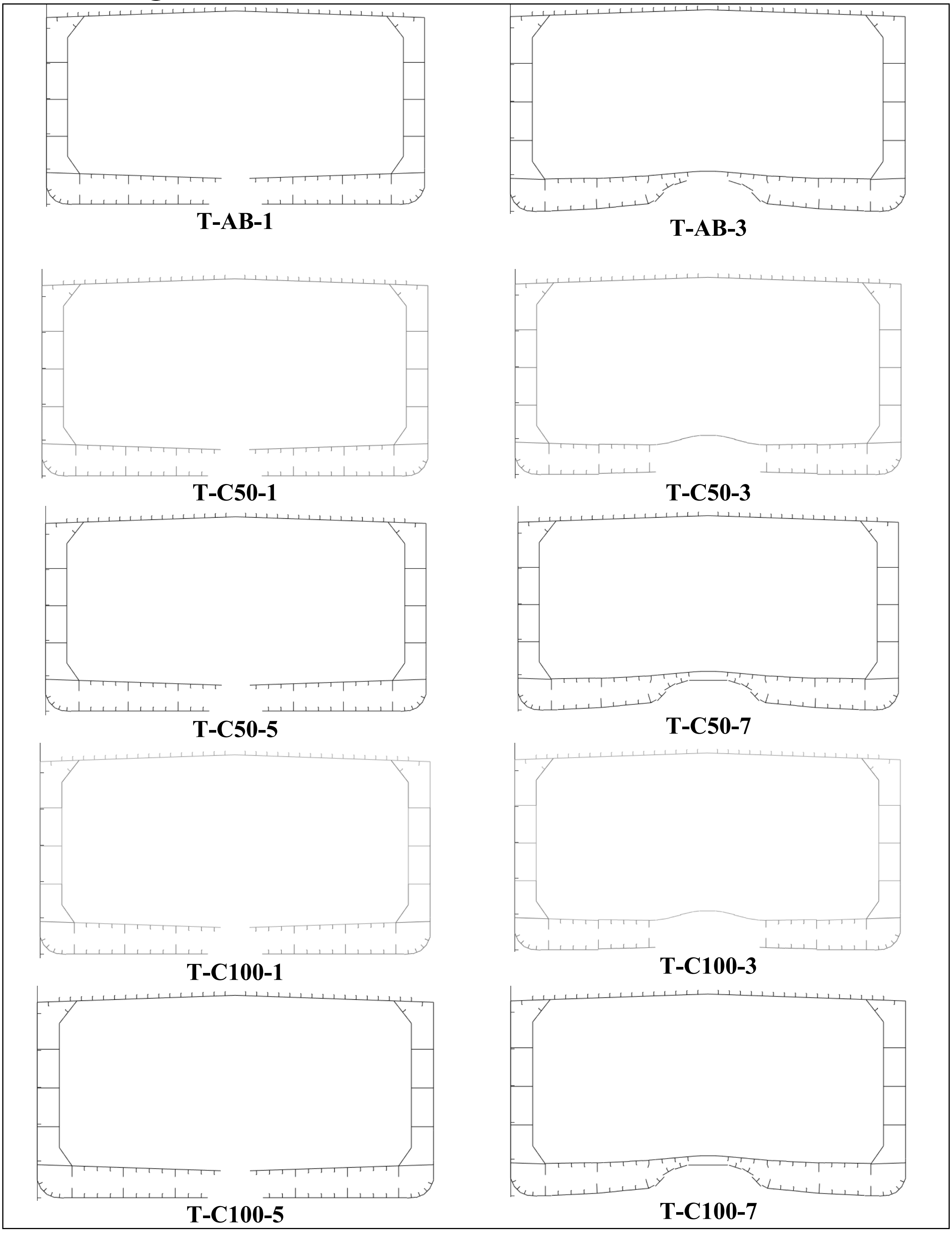

Figure A.1 Damaged cross sections used in the URSA code for the biaxial bending ULS analyses. Models are built up with hard corner, stiffener, and stiffened plate elements.

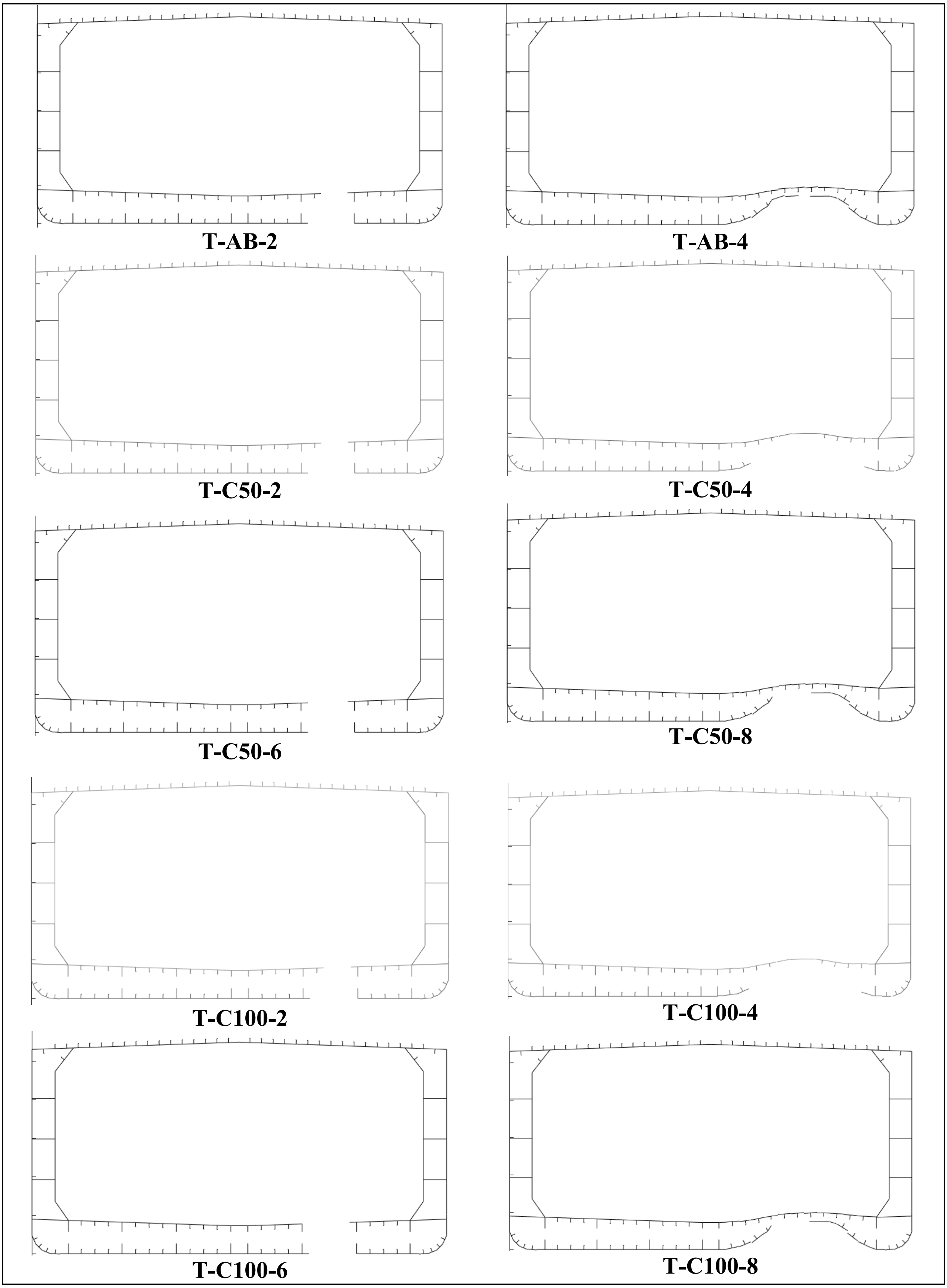

Figure A.2 Damaged cross sections used in the URSA code for the biaxial bending ULS analyses. Models are built up with hard corner, stiffener, and stiffened plate elements.